On the Formulation and Universality of Monin–Obukhov Similarity Functions for Mean Gradients and Standard Deviations in the Unstable Surface Layer: Results from Surface-Layer-Resolving Large-Eddy Simulations

BJÖRN MARONGA

Institut für Meteorologie und Klimatologie, Leibniz Universität Hannover, Hannover, Germany

JOACHIM REUDER

Geophysical Institute, University of Bergen, and Bjerknes Centre for Climate Research, Bergen, Norway

(Manuscript received 17 June 2016, in final form 16 November 2016)

ABSTRACT

Surface-layer-resolving large-eddy simulations (LESs) of free-convective to near-neutral boundary layers are used to study Monin–Obukhov similarity theory (MOST) functions. The LES dataset, previously used for the analysis of MOST relationships for structure parameters, is extended for the mean vertical gradients and standard deviations of potential temperature, specific humidity, and wind. Also, local-free-convection (LFC) similarity is studied. The LES data suggest that the MOST functions for mean gradients are universal and unique. The data for the mean gradient of the horizontal wind display significant scatter, while the gradients of temperature and humidity vary considerably less. The LES results suggest that this scatter is mostly related to a transition from MOST to LFC scaling when approaching free-convective conditions and that it is associated with a change of the slope of the similarity functions toward the expected value from LFC scaling. Overall, the data show slightly, but consistent, steeper slopes of the similarity functions than suggested in literature. The MOST functions for standard deviations appear to be unique and universal when the entrainment from the free atmosphere into the boundary layer is sufficiently small. If entrainment becomes significant, however, we find that the standard deviation of humidity no longer follows MOST. Under free-convective conditions, the similarity functions should reduce to universal constants (LFC scaling). This is supported by the LES data, showing only little scatter, but displaying a systematic height dependence of these constants. Like for MOST, the LFC similarity constant for the standard deviation of specific humidity becomes nonuniversal when the entrainment of dry air reaches significant levels.

1. Introduction

Monin–Obukhov similarity theory (MOST; Obukhov 1971; Monin and Obukhov 1954) of the atmospheric surface layer has been a widely accepted pragmatic framework in the scientific community for more than 50 years (Foken 2006). It provides empirical relationships between the atmospheric stability and nondimensionalized quantities in the surface layer when using a suitable set of scaling parameters. However, as MOST does not predict the precise formulation of these relationships, they have to be determined experimentally. The MOST framework has been tested and validated in numerous field experiments, with the Kansas and Minnesota experiments in 1968 and 1973 being the most famous ones (Businger et al. 1971; Kaimal et al. 1976; Kaimal and Wyngaard 1990). Nowadays, MOST is used in numerous meteorological models, for example, to determine the turbulent fluxes at the surface as boundary condition. It is also employed by experimentalists, for example, to derive surface fluxes of sensible and latent heat from scintillometer observations at elevated heights (e.g., Kohsiek et al. 2002; Meijninger et al. 2006; Evans et al. 2012). In the free-convection limit, local-free-convection (LFC) scaling provides a different and simpler set of scaling parameters.

According to MOST, the empirical relationships for nondimensionalized quantities, once formulated, must be unique. It is also commonly assumed that these

Corresponding author e-mail: Björn Maronga, maronga@muk.uni-hannover.de

DOI: 10.1175/JAS-D-16-0186.1

relationships are identical for thermal and moisture quantities when the correlation between (potential) temperature θ and (specific) humidity q is unity (Hill 1989). Experimental datasets, however, have revealed that such universal functions are difficult to obtain. Consequently, there coexist various ''universal'' functions in literature (see section 2). Some authors hypothesize that no universal functions, as demanded by MOST, exist at all, or they question the validity of MOST. Wilson (2008), for example, analyzed sonic anemometer data over a Utah salt flat and found that the neutral-limit value for the normalized standard deviation of vertical velocity deviated significantly from what is considered to be the standard value. McNaughton (2006) used a structural model of the atmospheric surface layer and found that the larger eddies of the boundary layer affect the surface layer so that a basic assumption of MOST is violated. Moreover, there is discussion on dissimilarity between the turbulent transport of heat and moisture that could affect the universality of MOST functions (Li et al. 2012a,b). Li et al. (2012a), for example, pointed out that dissimilarity between the turbulence transport of temperature and humidity occurred in their measurement data for weakly unstable conditions. Consequently, the MOST relationships for their observed structure parameters for temperature C_T^2 and humidity C_q^2 were found to differ significantly. They referred to the study of Hill (1989) and concluded that dissimilarity might be observed whenever the correlation between temperature and humidity is less than 1. Beyrich et al. (2005) showed that this can be a frequent feature within the surface layer. Li et al. (2012b) studied the dissimilarity between the turbulent transport of heat and momentum in terms of MOST functions theoretically and stated, in line with previous studies, that heat is generally found to be more efficiently transported than momentum. Katul et al. (2013) and Li et al. (2015), among others, revisited the MOST framework by relating turbulence spectra with the bulk flow properties.

One persisting issue in MOST is the theoretical consideration that LFC scaling predicts the slope of the MOST functions in the free-convection limit (Wyngaard et al. 1971; Businger 1973), but it has not been possible so far to find MOST functions that fulfill this requirement and follow the predicted slopes. Businger (1973) stated that this might be related to the fact that the requirement of the friction velocity u_* approaching zero is not fulfilled owing to production of wind shear by convective thermals.

Khanna and Brasseur (1997) were the first to employ turbulence-resolving large-eddy simulations (LESs) to study the predictability of the commonly used MOST functions for mean gradients, variances, budgets of turbulent kinetic energy, and temperature variance, as well as velocity and temperature spectra under unstable conditions. They found that the temperature field in the LES model satisfied MOST, while the velocity field showed significant deviations from the proposed functions. They also reported an indirect dependency of the boundary layer depth z_i on all MOST functions, except for temperature. Unfortunately, they did not propose new formulations of the similarity functions based on their LES data. Later, Johansson et al. (2001) used observations to support the findings of Khanna and Brasseur (1997) [see also comment and reply in Andreas and Hicks (2002) and Johansson et al. (2002)]. Steeneveld et al. (2005) used LES data and field measurements and came to the conclusion that both z_i and the entrainment flux ratio r could impact the corresponding MOST relationships. In a precursor to this paper, Maronga (2014, hereafter M14) employed surface-layer-resolving LES to investigate the similarity functions for C_T^2 and C_q^2 in the unstable surface layer. M14 derived new similarity functions based on the LES data and could show that these are no longer universal when entrainment of dry warm air from the free atmosphere into the boundary layer was significant. This was the case when the entrainment flux ratio for moisture $r_q \approx 1$. However, this effect was limited to C_q^2, as the entrainment flux ratios for sensible heat r_θ are usually much smaller so that entrained warm air usually does not impact the surface-layer structure to a significant amount. Moreover, it was found that neglecting the effect of humidity on stability is no adequate assumption and can alter the similarity relationships significantly. Kooijmans and Hartogensis (2016) recently derived the MOST functions for C_T^2 and C_q^2 based on 11 field measurement campaigns and showed that the proposed functions of M14 were in remarkable agreement with their best fits from the combined measurement dataset. Their result provides additional confidence in the use of LES data to derive and study MOST functions. Braam et al. (2014) showed that the fitting procedure itself affects the MOST functions for structure parameters and requires special attention.

Over the past years, direct numerical simulations have been employed to investigate MOST (e.g., van de Wiel et al. 2008; Chung and Matheou 2012). However, these studies have so far focused on flow regimes with stable static stability only, possibly owing to the fact that much larger model domains are required when simulating convective boundary layers.

As MOST is applied in almost all meteorological models, ranging from single-column models, microscale

models, LES with coarse grid (where the surface layer cannot be resolved), and numerical weather predictions models, the formulation and universality of the used MOST relationships is of major importance and contributes significantly to the quality of surface-layer parameterizations. In this context we want to investigate some major open questions regarding MOST that are present for some decades now.

In this paper, we will make use of the extensive LES dataset generated by M14 in order to extend the analysis for structure parameters to the commonly used relationships for mean gradients of θ, q, and horizontal wind velocity u_h. We will also study the standard deviations of θ, q, and of the vertical velocity w. Finally, we will derive new MOST functions for these quantities and determine free-convection scaling constants. Our main focus will not be to provide better MOST functions than already proposed in literature. Our focus will mainly be on the following basic scientific questions: (i) Is it possible to derive universal MOST functions from LES data? (ii) Does the concept of MOST collapse in free convection? (iii) Is it possible to unify MOST relationships and LFC scaling predictions for mean gradients in the free convection limit? (iv) Can dissimilarity between the turbulent transport of heat and moisture due to entrainment alter the similarity relationships?

The LES concept provides ideal conditions for answering these questions as it allows performing simulations with well-controlled parameters, such as prescribed surface fluxes, perfect horizontal homogeneity of the surface, and stationarity of the flow. Moreover, the LES technique allows to simultaneously perform virtual measurements at different height levels within the surface layer and spatial averaging can be used instead of the commonly used time averaging (and using Taylor's hypothesis of frozen turbulence) to improve statistics. The disadvantage is, however, that LES models generally suffer from numerical errors and effects of the small-scale turbulence parameterizations involved, particularly close to the surface. In contrast, field observations do not involve such numerical problems, but usually suffer from the lack of surface homogeneity, unsteadiness of the flow, sparse measurement density in space, and measurement uncertainty.

Despite the findings of former studies that suggested to incorporate both z_i and r (Steeneveld et al. 2005; Johansson et al. 2001), we will confine ourselves to the classic MOST formulation. The reasoning behind this is that, in most circumstances, the required information on the structure of the top of the boundary layer is not measured, but MOST is nonetheless used as a pragmatic solution.

The paper is organized as follows. Section 2 deals with the theoretical background of MOST and LFC scaling and the current state of the art. Section 3 gives a short overview on the LES database. The main results are presented in section 4, before we end with a summary and a short outlook in section 5.

2. Theory

a. Monin–Obukhov similarity theory

Under the assumption of horizontal homogeneity of the surface and a steady-state flow, MOST implies that the vertical turbulent fluxes within the lowest decameters of the atmosphere are, to a first-order approximation, constant with height (e.g., Andreas 1988; Hill 1989). The surface layer is commonly defined to be the lower part of the boundary layer, where vertical fluxes vary by less than 10% of their magnitude (Stull 1988). The relevant scaling parameters for MOST then are the measurement height z, the Obukhov length L, the near-surface kinematic fluxes of heat $\overline{w'\theta'}_0$ and moisture $\overline{w'q'}_0$, and u_*. The Obukhov length is defined as

$$L = -\frac{\overline{\theta}_v u_*^3}{\kappa g \overline{w'\theta'}_{v0}}, \tag{1}$$

where θ_v and $\overline{w'\theta'}_{v0}$ are the virtual potential temperature and near-surface buoyancy flux, respectively, g is the gravitational acceleration, and $\kappa = 0.4$ is the von Kármán constant. The overbar denotes an average (spatial average in this study) and the prime indicates the turbulent deviation from this average. The friction velocity is defined as

$$u_* = (\overline{w'u'}_0^2 + \overline{w'v'}_0^2)^{1/4}, \tag{2}$$

with $\overline{w'u'}_0$ and $\overline{w'v'}_0$ being the components of the vertical near-surface momentum flux and u and v being the horizontal wind components in x and y directions, respectively. Based on this set of parameters, there is an additional dimensionless group: z/L, which is commonly referred to as a stability parameter. Moreover, a temperature scale θ_* and a humidity scale q_* are given by

$$\theta_* = -\frac{\overline{w'\theta'}_0}{u_*} \quad \text{and} \tag{3}$$

$$q_* = -\frac{\overline{w'q'}_0}{u_*}. \tag{4}$$

Following MOST, any given quantity in the surface layer should follow a universal function that only depends on z/L, if properly scaled with θ_*, q_*, u_*, and z (e.g., Andreas 1988). The gradients of mean profiles of θ, q, and u_h in the surface layer should thus be describable by

$$\frac{\partial\theta}{\partial z}\frac{\kappa z}{\theta_*}=\phi_h\left(\frac{z}{L}\right), \tag{5}$$

$$\frac{\partial q}{\partial z}\frac{\kappa z}{q_*}=\phi_q\left(\frac{z}{L}\right), \quad \text{and} \tag{6}$$

$$\frac{\partial u_h}{\partial z}\frac{\kappa z}{u_*}=\phi_m\left(\frac{z}{L}\right). \tag{7}$$

Here, ϕ_h, ϕ_q, and ϕ_m should be unique functions of z/L. As MOST does not provide the exact formulation of these functions, they must be determined experimentally. While many authors have proposed functions for ϕ_h and ϕ_m (e.g., Businger et al. 1971; Dyer 1974; Dyer and Bradley 1982; Panofsky and Dutton 1984; Högström 1988; Kader and Yaglom 1990), it is usually assumed that $\phi_h=\phi_q$. However, Li et al. (2012b) demonstrated that a ''scale resonance'' between turnover eddies and deviations in the instantaneous temperature profiles can lead to enhanced heat transport under unstable conditions. Nowadays, the so-called Businger–Dyer (BD) form is commonly used, namely

$$\phi_h=\phi_m^2=C_1\left(1-C_2\frac{z}{L}\right)^{-1/2}, \tag{8}$$

with $C_1=1$ and C_2 being an empirical constant, for which different values have been reported in literature (e.g., Dyer and Bradley 1982; Panofsky and Dutton 1984). Note that some formulations also propose $C_1\neq 1$ and $\phi_h\neq\phi_m^2$ (e.g., Businger et al. 1971; Dyer 1974; Högström 1988). For a discussion and summary of proposed functions used today, see Högström (1988).

For standard deviations of temperature σ_θ, humidity σ_q, and vertical velocity σ_w, MOST predicts

$$\frac{\sigma_\theta}{\theta_*}=\phi_{\sigma_\theta}\left(\frac{z}{L}\right), \tag{9}$$

$$\frac{\sigma_q}{q_*}=\phi_{\sigma_q}\left(\frac{z}{L}\right), \quad \text{and} \tag{10}$$

$$\frac{\sigma_w}{u_*}=\phi_{\sigma_w}\left(\frac{z}{L}\right), \tag{11}$$

with the widely accepted similarity functions

$$\phi_{\sigma_\theta}=C_3\left(1-C_4\frac{z}{L}\right)^{-1/3}, \tag{12}$$

$$\phi_{\sigma_q}=C_5\left(1-C_6\frac{z}{L}\right)^{-1/3}, \quad \text{and} \tag{13}$$

$$\phi_{\sigma_w}=C_7\left(1-C_8\frac{z}{L}\right)^{1/3}, \tag{14}$$

with C_3–C_8 being constants, again with several different proposed values from literature (e.g., Liu et al. 1998; Andreas et al. 1998; Panofsky et al. 1977; Kaimal and Finnigan 1988; Wilson 2008).

b. Local-free-convection scaling

The Obukhov length can be regarded as the height where mechanical and buoyant production of turbulence are roughly in balance (Andreas 1991). When buoyant production dominates the generation of turbulence (that is the case in calm winds), the mean wind collapses to zero and $u_*\to 0$. Consequently, $L\to 0$ and can therefore no longer be used as a proper scaling parameter. Buoyancy then is the dominant forcing. Note that Businger (1973) and Schumann (1988) discussed that the thermals in free convection can create local wind shear of short duration, which implies that a shear production of turbulence remains that can in turn prevent u_* from being close to zero. Also at higher levels in the surface layer, buoyancy can dominate and the flow should behave as in true free convection. This is commonly referred to as LFC (e.g., Wyngaard et al. 1971).

In the free-convection limit, we can formulate a set of LFC scaling parameters:

$$w_{\mathrm{LF}}=\left(\frac{g}{\overline{\theta_v}}\overline{w'\theta'_v}_0 z\right)^{1/3}, \tag{15}$$

$$\theta_{\mathrm{LF}}=\frac{\overline{w'\theta'}_0}{w_{\mathrm{LF}}}, \tag{16}$$

and

$$q_{\mathrm{LF}}=\frac{\overline{w'q'}_0}{w_{\mathrm{LF}}}. \tag{17}$$

Due to the fact that the number of relevant variables equals the number of dimensions (z is the only variable with unit of length), there is only one dimensionless group and the dimensionless mean gradients should follow (Wyngaard et al. 1971)

$$\frac{\partial\theta}{\partial z}\frac{z}{\theta_{\mathrm{LF}}}=A_\theta, \tag{18}$$

$$\frac{\partial q}{\partial z}\frac{z}{q_{\mathrm{LF}}}=A_q, \quad \text{and} \tag{19}$$

$$\frac{\partial u_h}{\partial z}\frac{z}{w_{\mathrm{LF}}}=A_u, \tag{20}$$

where A_θ, A_q, and A_u are universal constants. Sorbjan (1986) found $A_\theta=-0.35$ based on the Minnesota 1973 data. To the authors' knowledge no value for A_q has been proposed so far. The LFC formulation for wind [Eq. (20)] is not meaningful, as the mean wind gradient

collapses to zero in the free-convection limit, but it can be used to derive the slope of the respective MOST function as will be discussed below (see also Businger 1973).

The nondimensional standard deviations according to LFC scaling read

$$\frac{\sigma_\theta}{\theta_{\mathrm{LF}}} = A_{\sigma_\theta}, \tag{21}$$

$$\frac{\sigma_q}{q_{\mathrm{LF}}} = A_{\sigma_q}, \quad \text{and} \tag{22}$$

$$\frac{\sigma_w}{w_{\mathrm{LF}}} = A_{\sigma_w}. \tag{23}$$

For A_{σ_θ}, values of 1.29–1.41 have been reported, whereas no suggestions are available for A_{σ_q}. The value of A_{σ_w} is believed to be 1.1–1.40 (Wyngaard et al. 1971; Sorbjan 1986; Caughey and Readings 1975; Kaimal et al. 1976; Shao and Hacker 1990; Khanna and Brasseur 1997).

Wyngaard et al. (1971) and Businger (1973) showed that the LFC framework provides predictions of the slope of the MOST functions by looking at the free-convection limit (i.e., $-z/L \to \infty$). LFC then predicts for mean gradients that $\phi_h \sim (-z/L)^{-1/3}$, $\phi_q \sim (-z/L)^{-1/3}$, and $\phi_m \sim (-z/L)^{1/3}$. For standard deviations, LFC predicts $\phi_{\sigma_\theta} \sim (-z/L)^{-1/3}$, $\phi_{\sigma_q} \sim (-z/L)^{-1/3}$, and $\phi_{\sigma_w} \sim (-z/L)^{1/3}$ for large values of $-z/L$. The MOST formulations for standard deviations [see Eqs. (12)–(14)] indeed follow this prediction. As a consequence, the LFC constants can also be determined from the MOST formulations as

$$A_{\sigma_\theta} = -C_3 C_4^{-1/3} \kappa^{-1/3}, \tag{24}$$

$$A_{\sigma_q} = -C_5 C_6^{-1/3} \kappa^{-1/3}, \quad \text{and} \tag{25}$$

$$A_{\sigma_w} = C_7 C_8^{1/3} \kappa^{1/3}. \tag{26}$$

For mean gradients, however, experimental data has shown that ϕ_θ and ϕ_m rather follow a power law of $-1/2$ and $-1/4$ instead of $-1/3$ and $1/3$, respectively (e.g., Wyngaard et al. 1971; Businger 1973). Note that for ϕ_m this implies that the slope should have the opposite sign than what is observed in measurement data ($-1/4$ slope). In the BD form ($\phi_h \neq \phi_m^2$), the LFC prediction $\phi_h \sim (-z/L)^{-1/3}$ leads to $\phi_m \sim (-z/L)^{-1/6}$, which is not compatible with the predicted 1/3 slope derived directly from LFC scaling. Some authors have subsequently tried to derive ϕ_m functions that follow the $-1/6$ power law (e.g., Delage and Girard 1992; Fairall et al. 1996). There also exist suggestions with a slope of $-1/3$ (Carl et al. 1973; Wilson 2001). To our knowledge, it has not been possible to find solid relationships between the LFC constants and the constants used in the MOST similarity functions for mean gradients so far. Businger (1973) discussed that the LFC prediction must not necessarily be fulfilled when using MOST, as true free convection is never reached near the surface, for example, as a result of local shear production from horizontal winds induced by thermals (see above).

3. LES model and case description

a. *LES model*

The Parallelized Large-Eddy Simulation Model (PALM, revision 893) (Raasch and Schröter 2001; Maronga et al. 2015) has been used for the present study. It has been widely applied to study different flow regimes in the convective and neutral boundary layer (e.g., Raasch and Franke 2011; Letzel et al. 2008). All simulations were carried out using cyclic lateral boundary conditions. The grid was stretched in the vertical direction well above the top of the boundary layer to save computational time in the free atmosphere.

MOST was applied locally between the surface and the first computational grid level (''local similarity model''; see also Peltier and Wyngaard 1995) to calculate the local friction velocity u_* from the roughness length and the local wind profiles [see also Panofsky and Dutton (1984), chapter 6.5]. PALM uses the stability functions after Panofsky and Dutton (1984). Note that the use of MOST as boundary condition is limited to the calculation of u_* based on the near-surface wind profile and the given stability functions, while surface fluxes of heat and moisture are explicitly prescribed at the surface. There is thus a possibility that the calculated u_* values might contain a small uncertainty, depending on the exact MOST functions used as boundary condition. From our experience, this uncertainty is only small and should thus not affect the LES results significantly. This is particularly true as the model itself does not ''feel'' the underlying MOST function but reacts directly to the calculated u_*. The flow is thus in balance with the surface momentum fluxes given by u_*.

A 1.5-order flux–gradient subgrid closure scheme after Deardorff (1980) was applied in the formulation of Saiki et al. (2000), which requires the solution of an additional prognostic equation for the subgrid-scale (SGS) turbulent kinetic energy. A fifth-order advection scheme of Wicker and Skamarock (2002) and a third-order Runge–Kutta time step scheme (Williamson 1980) were used to discretize the model in space and time. In case of a prescribed geostrophic wind, a one-dimensional version of the model with fully parameterized turbulence, using a mixing-length approach after Blackadar (1997) and stationary temperature and humidity profiles, was used for precursor simulations over

TABLE 1. Overview of the LES setup (reproduced from M14), complemented by the maximum values of z_i as well as entrainment flux ratios for sensible heat r_θ, moisture r_q, and buoyancy r_{θ_v} that have been determined from the LES data; β_0 is the surface Bowen ratio and γ is lapse rate of potential temperature in the capping inversion.

Case	Wind ($m\,s^{-1}$)	$\overline{w'\theta'}_0$ ($K\,m\,s^{-1}$)	$\overline{w'q'}_0$ ($g\,kg^{-1}\,m\,s^{-1}$)	β_0	γ ($K\,km^{-1}$)	r_θ	r_q	r_{θ_v}	$z_{i,\max}$ (km)
W00	0	0.075	0.11	0.27	27	−0.25	0.3	−0.15	1.08
W02	2	0.075	0.11	0.27	27	−0.25	0.35	−0.15	1.08
W04	4	0.075	0.11	0.27	27	−0.25	0.3	−0.15	1.08
W06	6	0.075	0.11	0.27	27	−0.25	0.3	−0.15	1.08
W08	8	0.075	0.11	0.27	27	−0.2	0.3	−0.15	1.08
W10	10	0.075	0.11	0.27	27	−0.2	0.3	−0.15	1.08
W10_F50	10	0.0375	0.055	0.27	27	−0.3	0.3	−0.15	1.04
W10_F10	10	0.0075	0.011	0.27	27	−0.4	0.3	−0.2	1.0
W10_F00	10	0.0000	0.000	—	27	$-\infty$	∞	$-\infty$	1.0
W00_dry	0	0.075	0.0	∞	27	−0.15	—	−0.15	1.06
W00_β05	0	0.075	0.6	0.05	27	−0.6	0.2	−0.15	1.14
W00_β40	0	0.109	0.11	0.4	27	−0.2	0.4	−0.15	1.11
W00_γ07	0	0.075	0.11	0.27	7	−0.3	1.0	−0.15	1.29
W08_dry	8	0.075	0.0	∞	27	−0.15	—	−0.15	1.06
W08_β05	8	0.075	0.6	0.05	27	−0.55	0.2	−0.15	1.14
W08_β40	8	0.109	0.11	0.4	27	−0.2	0.4	−0.15	1.11
W08_γ07	8	0.075	0.11	0.27	7	−0.3	1.0	−0.10	1.28

several days to generate steady-state wind profiles as initialization for the LES. Simultaneously, inertial oscillations in the near-neutral cases were effectively damped in the precursor simulations so that a steady state could be reached early in the LES runs.

b. Case description

The set of LES that was generated and described by M14 and is based on a reference simulation for the Cabauw area in the Netherlands from the study of Maronga et al. (2013). Details of the observed case are described in de Arellano et al. (2004). The model was discretized in space with 2048 grid points in each horizontal and 832 grid points in the vertical direction. The grid spacing was 4 m × 4 m × 2 m ($\Delta_x \times \Delta_y \times \Delta_z$). The simulations were driven by constant kinematic surface fluxes of heat and moisture with a Bowen ratio β_0 around 0.27. This relatively small Bowen ratio is due to the very wet soil in Cabauw with a groundwater table usually less than 2 m. A roughness length of 0.1 m was used. Neutrally stratified initial profiles of temperature (298 K) and humidity ($12\,g\,kg^{-1}$) with a capping inversion starting at $z = 950$ m and a depth of 250 m, and the stably stratified dry free atmosphere above with a lapse rate of $7\,K\,km^{-1}$ were prescribed. The lapse rates in the capping inversion are provided in Table 1. A detailed description of the setup can be found in Maronga et al. (2013, section 3 and Table 1, case A).

Based on this setup, the geostrophic wind speed and the prescribed surface fluxes were systematically varied for each simulation. This was done in order to generate a set of simulations (herein also referred to as reference simulations) that cover a large range of $-z/L$ for near-neutral to free-convective conditions. First, the geostrophic wind was increased from 0 to $10\,m\,s^{-1}$. Second, in order to cover those cases that are dominated by shear production ($-z/L < 0.1$), the surface fluxes were reduced to 50% and 10% of their initial values, based on the simulation with a background wind of $10\,m\,s^{-1}$. We complemented the dataset by a run with a background wind of $10\,m\,s^{-1}$ and zero surface fluxes to mimic an almost neutral boundary layer (as entrainment of warm and dry air is still possible). For sensitivity studies, β_0 was varied to values of 0.05 and 0.4 as well as ∞ (dry simulation). Furthermore, the lapse rate of temperature in the capping inversion γ was reduced for one case in order to study whether entrainment of warm and dry air affects the similarity functions. Because of the high computational costs these sensitivity cases were simulated for two selected background wind speeds only: $0\,m\,s^{-1}$ (free convection) and $8\,m\,s^{-1}$. The full list of simulations with the relevant parameters is given in Table 1.

c. Database and processing

Each simulation ran for 2 h. A quasi-steady state had reached in the surface layer for each run after at most 1 h of simulation time. Horizontally averaged profiles (spatial average over 2048^2 grid points) of temperature, humidity, and horizontal wind were thus output every 120 s during the second hour of the simulation. In addition, the (horizontal) variance profiles of temperature, humidity, and vertical wind were stored. The mean gradients of θ, q, and u_h were calculated for each vertical

grid level from the horizontally averaged profiles using central finite differences on the smallest scale (i.e., $2\Delta_z$). MOST and LFC scaling parameters were calculated from the prescribed surface fluxes and the time series of the horizontal mean u_* as calculated by PALM. For the calculation of L, the mean vertical profile of θ_v and the time series of the buoyancy flux were used. As θ_v was calculated from the prognostic variables θ and q as a three-dimensional quantity in PALM, the buoyancy flux was a direct model output.

The boundary layer depth (see Table 1) was defined as the height where the gradient of the horizontally averaged potential temperature had a maximum. Moreover, this height had to fulfill the requirement that the gradient was at least $0.002\,\mathrm{K\,m^{-1}}$ and greater than that of the four grid levels above. The value of z_i was in most cases in the order of 1 km. The top of the surface layer z_{SL} was taken as $0.1z_i$. M14 showed that this choice did not introduce any error.

Nondimensional mean gradients and standard deviations according to MOST and LFC were calculated in a postprocessing for each available time step and each height level within the surface layer. M14 explained that the surface layer could not be resolved sufficiently within the lowest seven grid points owing to the LES numerics [in agreement with the former LES of Khanna and Brasseur (1997) and Brasseur and Wei (2010)], but he showed that the nondimensionalized LES data for structure parameters collapsed to single curves when excluding data from these lowest grid levels (see his Fig. 2). In the present study we thus decided to remove the lowest seven grid points directly from our analysis.

MOST fitting functions are derived using the classical nonlinear least squares regression method. The data were not weighted; that is, regions with more data points led to an increased weighting for this region during the regression. Braam et al. (2014) studied the effect of the regression method, scaling, and weighting of the data on MOST fitting functions for structure parameters. From their results, they concluded that orthogonal regression would be more appropriate than classical least squares regression because uncertainties in the independent variables would be considered. They also suggested performing the regression on logarithmized data. However, their results are based on datasets from field observations that traditionally display large scatter, so that these specific details of the regression analysis indeed can have a strong impact. When scatter in the data is small, these impacts will be negligible. In section 4 we will see that the LES data in most cases indeed displays significantly less scatter than observational data so that we feel confident that our regression method does not imply uncertainties that we could overcome with an adjusted regression method as proposed by Braam et al. (2014).

4. Results

a. General features of the simulated boundary layers

After having reached a steady state (≈1-h simulation time), all cases displayed classical convective boundary layer profiles with a shallow, highly unstable region close to the surface, a well-mixed layer that extended up to a capping inversion, and the stably stratified and dry free atmosphere above (see Fig. 1 of M14). The profiles of $\overline{w'\theta'}_0$ displayed a linear decrease with height (not shown). In general, z_i was about 1.1 km (see Table 1). In the course of the simulations, the surface heating and turbulent mixing were not strong enough to tear down the capping inversion. The lapse rate within the capping inversion was thus a relevant parameter that steered the amount of entrainment of dry and warm air into the boundary layer, whereas the lapse rate in the free atmosphere was of minor importance. In the reference cases, r_θ and r_q displayed values around −0.25 and 0.3, respectively. Entrainment is thus small compared to the surface forcing. Cases W10_F50 and W10_F10 showed a somewhat lower z_i (1.04 and 1.0 km, respectively) because of a reduced surface forcing so that thermals were weaker and not able to penetrate the capping inversion as rigorously as in the reference cases. Sensitivity cases W00_γ07 and W08_γ07 (weak capping inversion) are characterized by a significantly increased z_i of up to 1.29 km. The entrainment flux ratio here is about −0.3 for temperature and 1.0 for moisture, showing that the entrainment flux (causing a drying of the boundary layer) became the same magnitude as the surface forcing (causing a moistening of the boundary layer), whereas no increase in the entrainment of sensible heat was present. M14 showed that this had a distinct effect on the similarity function for C_q^2. For a summary of all z_i values and the entrainment flux ratios, see Table 1.

In the following, we will derive MOST and LFC functions based on LES data. First, however, we should recognize that the LES technique aims at modeling reality, but it hardly gives a perfect image of nature (e.g., owing to the turbulence parameterization or numerical errors). The similarity functions to be derived in the following should thus be regarded as the "model truth" but might be somewhat different from what we must expect in the field. The obvious advantage of LES is that we can control the boundary conditions for the simulations very precisely. Key issues for field experiments,

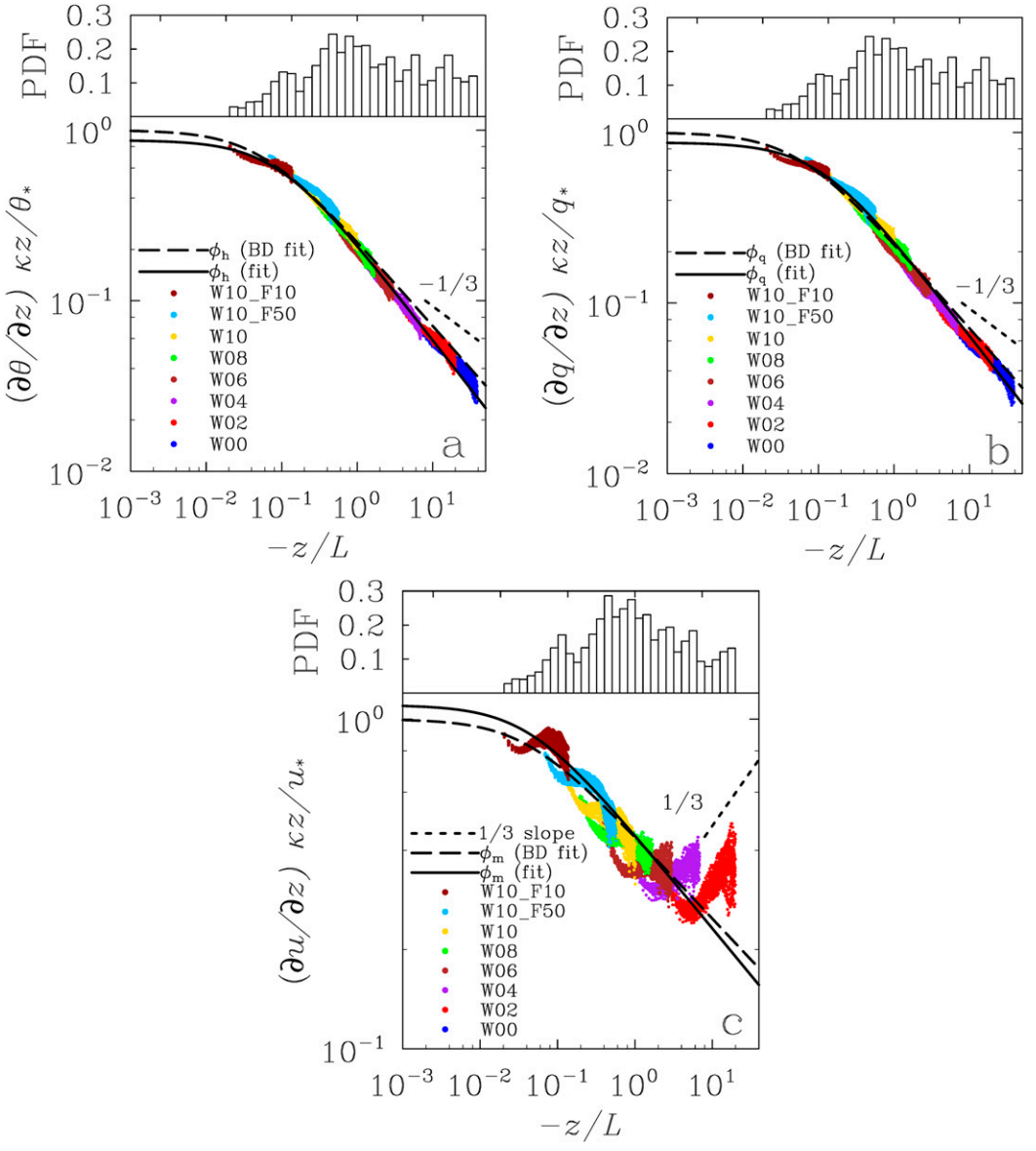

FIG. 1. (a) (bottom) Normalized mean gradients of temperature against stability parameter $-z/L$. The black solid line indicates the determined MOST fitting function, the black dashed line indicates the best fit using the BD formulation, and the black short-dashed line displays the predicted slope from LFC scaling. (top) The probability density function or $-z/L$ values that were used to determine the fitting function. (b),(c) As in (a), but for humidity and the horizontal wind component, respectively.

like surface heterogeneity and unsteadiness of the flow, are not present. Also we do not need to deal with problems of measurement uncertainty and we can replace the commonly used time average in field experiments by the more straightforward horizontal average to derive mean quantities.

b. MOST relationships for mean gradients

The nondimensional mean (horizontally averaged) gradients of θ, q, and u_h were calculated for the reference simulations after Eqs. (5)–(7) for all available time steps. Figure 1 shows these data against stability $-z/L$.

1) MEAN TEMPERATURE AND HUMIDITY GRADIENTS

Figures 1a and 1b show that the data points collapse to a single curve with remarkably little scatter in the data. As L remains rather constant during each simulation, the variations in $-z/L$ for each case refer to changes in the measurement height. We observe neither

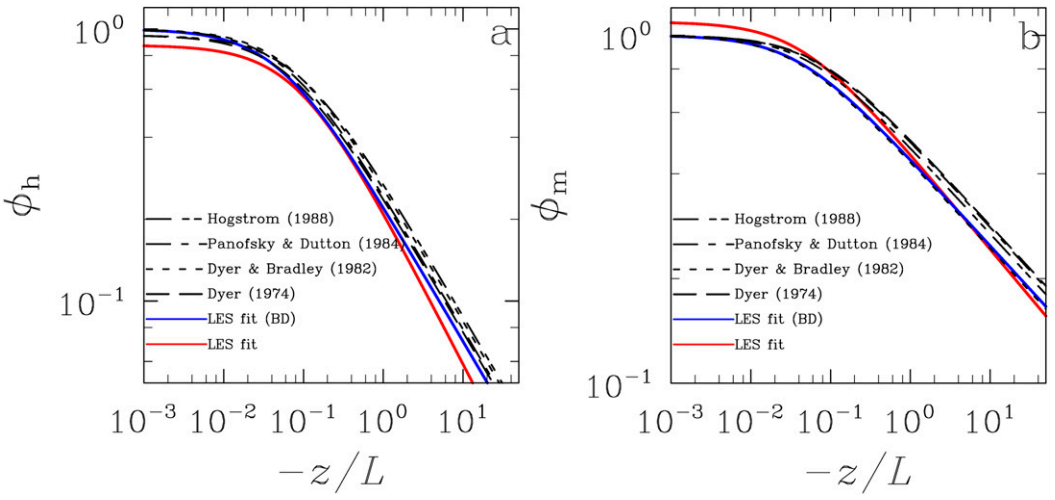

FIG. 2. Overview of fitting functions (a) ϕ_θ and (b) ϕ_m that have been proposed in literature against stability parameter $-z/L$ and compared to the LES fit (red solid lines) and the LES fit using the BD formulation (solid blue lines).

significant scatter due to variation in time nor due to a variation in height. From the fact that the data points from the different cases overlap to a great extent, we can conclude that a variation in z has basically the same effect on the dimensionless gradients as a variation in L. This is in agreement with the findings for structure parameters in the precursor of this study (see M14).

From the data points, we calculated two different fitting functions: the commonly accepted BD formulation [see Eq. (8)], assuming a power law of $-1/2$ as well as a neutral limit of unity, and a new fitting function where the coefficients and the power-law exponents all were free parameters. These fitting functions read

$$\phi_h = \left(1.0 - 19.7\frac{z}{L}\right)^{-0.5} \quad \text{(Businger–Dyer)}, \tag{27}$$

$$\phi_h = 1.1\left(1.5 - 17.0\frac{z}{L}\right)^{-0.57} \quad \text{(new)}, \tag{28}$$

$$\phi_q = \left(1.0 - 18.5\frac{z}{L}\right)^{-0.5} \quad \text{(Businger–Dyer), and} \tag{29}$$

$$\phi_q = 1.1\left(1.5 - 14.5\frac{z}{L}\right)^{-0.57} \quad \text{(new)}. \tag{30}$$

From these formulations we can infer that the commonly assumed relation $\phi_h \approx \phi_q$ seems to be reasonable, even though our functions are not fully identical. Moreover, we note that the LES data suggest a slightly steeper slope of the ϕ functions than the commonly used $-1/2$ in the BD form. Otherwise, the suggested shape of the fitting functions is very well met. Furthermore, it is noteworthy that even the data of case W00 (true free convection) behaves according to MOST. While this might be somehow surprising, it clearly supports the argument of Businger (1973) and Schumann (1988) that the large eddies in a buoyancy-driven boundary layer create a local wind shear that, when averaged, yields a friction velocity larger than zero. In our simulation data we observe $u_* \approx 0.2\,\mathrm{m\,s^{-1}}$, which is in agreement with the reasoning of Businger (1973). What is indeed positively surprising is that these data behave according to MOST scaling.

As LFC scaling would suggest the slope of the fitting functions to be $-1/3$ instead of $-1/2$, Figs. 1a and 1b were complemented by a line indicating the $-1/3$ slope. It is visible that the LES data do not back up this behavior for most of the $-z/L$ range. However, for large values of $-z/L \geq 8$, we see that the data indeed align along the slope predicted by LFC scaling. This result suggests that there is indeed a transition region where MOST and LFC scaling are blending. The commonly used formulations for ϕ_h and ϕ_q inherently fail to reproduce this transition as only a single slope can be prescribed. More elaborated formulations that incorporate the "kink" in the slope around $-z/L = 8$ might overcome this problem in the future.

Figure 2a shows the derived fitting functions ϕ_h in comparison with a selection of functions proposed in literature. Note that we used the modified functions for a von Kármán constant of 0.4 given by Högström (1988) throughout the present study (see also Table 2). The LES fitting functions predict slightly smaller values of the dimensionless temperature gradient, particularly for very unstable conditions (cf. fitting functions of Dyer 1974; Dyer and Bradley 1982; Panofsky and Dutton 1984; Högström 1988). Nevertheless, the overall agreement is good and the data fits best against the proposed

TABLE 2. Overview of MOST functions proposed in literature. The formulations have been partly modified for use with $\kappa = 0.4$ after Högström (1988).

Reference	ϕ_h	ϕ_q	ϕ_m	ϕ_{σ_θ}	ϕ_{σ_q}	ϕ_{σ_w}
Dyer (1974)	$0.95\left(1-15.2\frac{z}{L}\right)^{-0.5}$	—	$1.0\left(1-15.2\frac{z}{L}\right)^{-0.25}$	—	—	—
Dyer and Bradley (1982)	$1.0\left(1-14.0\frac{z}{L}\right)^{-0.5}$	—	$1.0\left(1-28.0\frac{z}{L}\right)^{-0.25}$	—	—	—
Panofsky and Dutton (1984)	$1.0\left(1-16.0\frac{z}{L}\right)^{-0.5}$	—	$1.0\left(1-16.0\frac{z}{L}\right)^{-0.25}$	—	—	—
Högström (1988)[a]	$0.95\left(1-11.6\frac{z}{L}\right)^{-0.5}$	—	$1.0\left(1-19.0\frac{z}{L}\right)^{-0.25}$	—	—	—
Wyngaard et al. (1971)	—	—	—	$-0.65\left(\frac{z}{L}\right)^{-1/3}$	—	—
Liu et al. (1998)	—	—	—	$-2.0\left(1-8\frac{z}{L}\right)^{-1/3}$	—	—
Andreas et al. (1998)	—	—	—	$-3.2\left(1-28.4\frac{z}{L}\right)^{-1/3}$	$-4.1\left(1-28.4\frac{z}{L}\right)^{-1/3}$	$1.2\left(0.7-3\frac{z}{L}\right)^{1/3}$
Panofsky et al. (1977)	—	—	—	—	—	$1.3\left(1.0-3\frac{z}{L}\right)^{1/3}$
Kaimal and Finnigan (1988)	—	—	—	—	—	$1.25\left(1.0-3\frac{z}{L}\right)^{1/3}$
Wilson (2008), type a	—	—	—	—	—	$1.0\left(1.0-4.5\frac{z}{L}\right)^{1/3}$
Wilson (2008), type b	—	—	—	—	—	$0.8\left(1.0-9.5\frac{z}{L}\right)^{1/3}$
This study	$1.0\left(1-19.7\frac{z}{L}\right)^{-0.5}$	$1.0\left(1-18.5\frac{z}{L}\right)^{-0.5}$	$\left(1.0-26.2\frac{z}{L}\right)^{-0.25}$	$-2.1\left(1-9\frac{z}{L}\right)^{-1/3}$	$-2.1\left(1-8\frac{z}{L}\right)^{-1/3}$	$1.0\left(1.0-4.1\frac{z}{L}\right)^{1/3}$
This study (new power law)	$1.1\left(1.5-17.0\frac{z}{L}\right)^{-0.57}$	$1.1\left(1.5-14.5\frac{z}{L}\right)^{-0.57}$	$0.85\left(0.4-9.5\frac{z}{L}\right)^{-0.285}$	$-1.2\left(0.2-1.7\frac{z}{L}\right)^{-0.4}$	$-1.2\left(0.2-1.6\frac{z}{L}\right)^{-0.4}$	—

[a] Modification of the function after Businger et al. (1971) for $\kappa = 0.40$.

function of Dyer (1974). The new LES fit suggests a neutral limit value of around 0.87, which is somewhat lower than the BD value of 1, but then we have no data points for small values of $-z/L < 0.02$, and the probability density functions show that significantly less values enter the fitting procedure for $-z/L < 0.1$ (see Figs. 1a,b). Therefore, we must admit that the neutral limit is not very well covered by the LES data. Moreover, the BD fit seems to compare better to previously suggested functions under unstable conditions, but it does not resemble the LES data for large values of $-z/L$ (cf. Fig. 1a).

2) MEAN HORIZONTAL WIND GRADIENT

The nondimensional mean horizontal wind gradients are shown in Fig. 1c. It is obvious that there is much more scatter in the data than for the temperature and humidity gradients. In more detail, we see that there is a clear height dependency of the data, as L remains constant during each run as already noted above. At low levels, the wind gradients show smaller values than expected by MOST, whereas higher levels display a clear overestimation. For highly unstable cases (W04 and W02) we observe additional scatter that is not related to a height dependency. This finding is in agreement with the former LES study of Khanna and Brasseur (1997), who also found significant departures of the velocity field from MOST, whereas temperature behaved much better. The dependence of the data on height is possibly related to deficiencies of the LES model in capturing the near-surface wind profile accurately. Such behavior was previously reported in literature (e.g., Andren et al. 1994; Sullivan et al. 1994) and is commonly ascribed to effects of the subgrid-scale model that plays an important role close to the surface. To minimize these effects, we cut off the lowest seven grid levels as already mentioned. Figures 1a,b reveal that the same effect is visible for the scalars, even though it is much less pronounced. Another reason could be the fact that MOST itself is a known oversimplification of the surface layer structure. In particular, the assumption of a constant flux layer is known to be a rough approximation and might lead to height-dependent nondimensionalized gradients. Despite this height dependency and the implied scatter in the data, Fig. 1c shows that the data do nevertheless group along a single line. The scatter involved compares to that of random errors reported in observations (e.g., Johansson et al. 2001) so that we are confident that the LES data are well suited to derive MOST relationships, even though the uncertainty in the functions will be larger than for the scalar gradients. Note also that no data points are visible for case W00 owing to the fact that the mean wind gradient here collapses to zero and is no longer a meaningful quantity. Consequently, it is difficult to derive suitable MOST fitting functions from these data. The best fits read

$$\phi_m = \left(1.0 - 26.2\frac{z}{L}\right)^{-0.25} \quad \text{(Businger–Dyer)} \quad \text{and} \quad (31)$$

$$\phi_m = 0.85\left(0.4 - 9.5\frac{z}{L}\right)^{-0.285} \quad \text{(new)}. \quad (32)$$

In the above "new" equation [Eq. (32)], we fixed the near-neutral limit to $\phi_m = 1.11$, which we obtained from W10_F00 by vertical averaging over all available time steps and height levels in the surface layer. This neutral limit values is slightly larger than unity as would follow from MOST. Possible explanations for this higher value are again deficiencies of the LES model in capturing the wind profile near the surface due to subgrid-scale modeling and the assumption of a constant flux layer in MOST. Also, note that we used $\kappa = 0.40$ throughout our analyses, but values of $\kappa = 0.4 \pm 0.04$ have been reported in literature (Högström 1996; Foken 2006). Businger et al. (1971), for example, first obtained a von Kármán constant of 0.35, based on the finding that $\phi_m = 1.15$ when using $\kappa = 0.4$. In that context, our finding that $\phi_m = 1.11$ in the neutral limit would suggest that $\kappa = 0.36$, which would be within the uncertainty range reported in literature and thus can be considered to be a realistic estimate.

Because of the significant scatter in Fig. 1c, it is difficult to judge which of the above functions performs better. As for the gradients of the scalars, we have complemented Fig. 1c by a line with a slope of 1/3, which would be the local-free-convection prediction (Businger 1973). Amazingly, the slope of the nondimensional wind gradients approaches the 1/3 slope for $-z/L \geq 8$. These results let us hypothesize that the larger scatter in the wind gradient data near free convection, in comparison with the scalar gradient data, can be to a large part explained by the fact that the sign of the slope must change within the transition from MOST to LFC scaling. To our knowledge this transition region from MOST to LFC scaling was not observed before, which can possibly be explained by the simple fact that not enough reliable data were present for $-z/L \geq 8$.

This interesting result might explain two key issues of past research on MOST: first, the fact that the traditional MOST fitting functions do not back up LFC scaling when looking at the free-convection limit, and second, the larger scatter observed in the mean wind gradient compared to the scatter in mean scalar gradients, at least near free-convective conditions.

Despite the large scatter, Fig. 2b shows that the ϕ_m functions from the LES data are well within the range of the proposed functions from literature (cf. Dyer 1974; Dyer and Bradley 1982; Panofsky and Dutton 1984; Högström 1988). The BD fit for the LES data is in

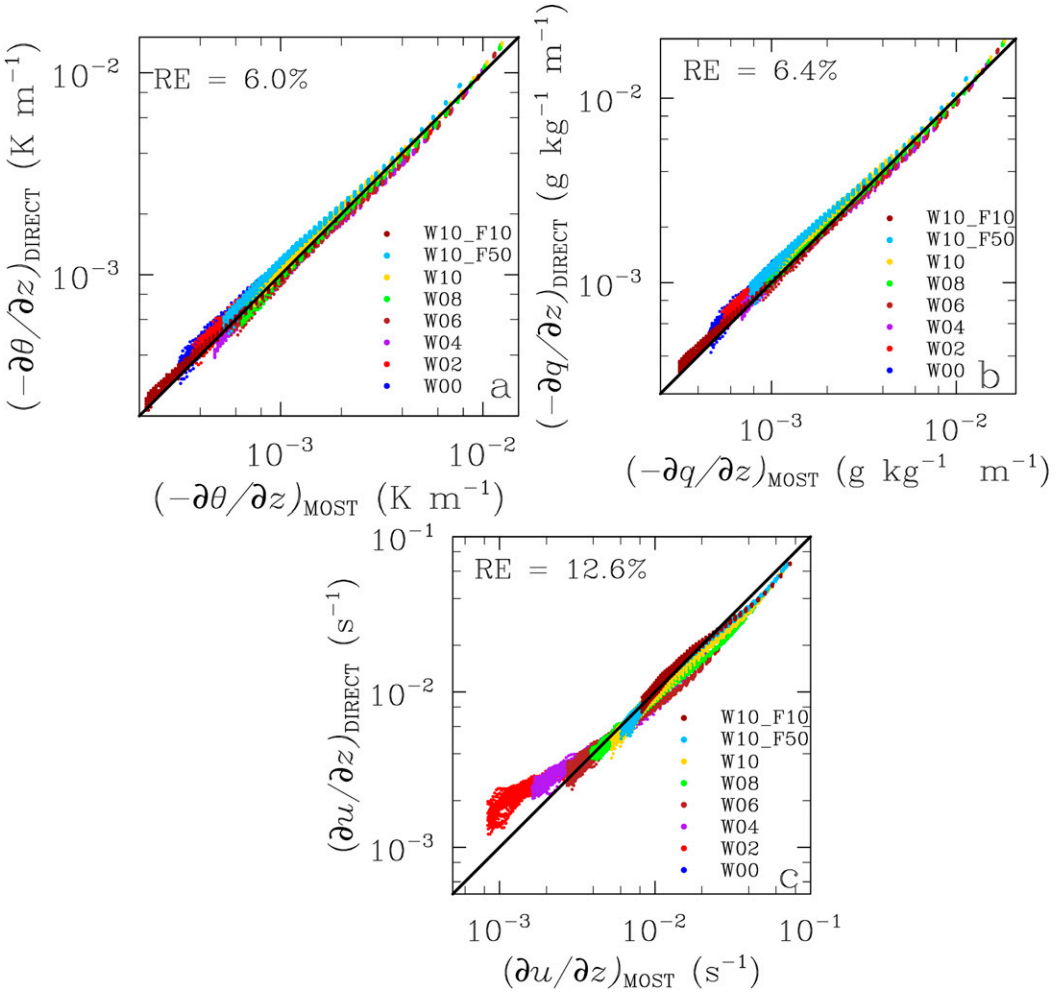

FIG. 3. Mean gradients of (a) temperature, (b) humidity, and (c) the horizontal wind velocity derived from the new MOST fitting functions against directly calculated values from the LES data. The relative error (RE) of the MOST results in relation to the directly measured data is listed in each frame.

remarkable agreement with the function after Dyer and Bradley (1982). The new LES fit again would also suggest lower values of ϕ_m for very unstable situations.

In summary, we must acknowledge that the BD fitting functions from the LES data are in much better agreement with those proposed in literature than the new fitting functions. However, they do not capture the steeper slope in the LES data for $-z/L > 0.1$ adequately. Here, the new fitting functions with an adjusted power law perform better.

3) SPURIOUS CORRELATIONS

In a comment on the paper of Johansson et al. (2001), Andreas and Hicks (2002) pointed out that spurious self-correlation cannot be avoided when using MOST scaling, because u_* appears on both axes of the scaled mean gradients. They showed that random errors in u_* will move a measured z/L–ϕ_m pair normal to the fitting function, whereas a $z/L - \phi_h$ pair will move along the fitting function under unstable conditions. They conclude that the larger scatter observed in ϕ_m might thus be the result of spurious correlations. In the reply to this comment, however, Johansson et al. (2002) state that also errors in θ_* should be considered, which adds additional scatter and makes the effect of spurious correlations less straightforward.

To check whether our newly derived fitting functions suffer from self-correlation, we followed the approach of Hartogensis and De Bruin (2005) and calculated the mean gradients indirectly using the new MOST fitting functions and directly from the raw LES data. As u_* and θ_* now appear only in the indirect calculation of the gradients, this approach allows for testing the new fitting functions without suffering from spurious correlations. These data are compared in Fig. 3 and show that the gradients of temperature and humidity compare remarkably well.

Only little scatter is observed and the relative error is around 6% and thus small, which lets us conclude that our fitting functions ϕ_h and ϕ_q do not suffer from self-correlation. The same holds for the mean wind gradient, even though we notice an systematical underestimation for gradients less than $6 \times 10^{-3}\,\mathrm{s}^{-1}$. This is related to the scatter we have seen for large values of $-z/L \geq 8$ in Fig. 1c (transition region from MOST to LFC scaling) and leads to a higher, but still reasonable, relative error of 12.6%. As for the gradients of the scalar, we do not see additional scatter in the data for the wind gradient, suggesting that spurious correlations are not affecting the MOST function and do not explain the larger scatter observed in Fig. 1c.

4) Turbulent Prandtl number

The turbulent Prandtl number (Pr_t), a nondimensional number, describes the ratio of turbulent transport of momentum to that of sensible heat (e.g., Li et al. 2015). In terms of MOST, Pr_t is defined as

$$\mathrm{Pr}_t = \frac{\phi_h}{\phi_m}. \tag{33}$$

It is often assumed that $\mathrm{Pr}_t = 1$, arguing that the same eddies are responsible for both exchange of momentum and heat, even though observations have suggested that $\mathrm{Pr}_t = 0.74$–1.0 (Kays 1994; Foken 2006). It is also expected that Pr_t is constant in the atmospheric surface layer. Several studies have revealed, however, that Pr_t displays significant variability depending on stability of the flow. Figure 4 shows Pr_t, calculated directly from the LES data as well as derived from the new fitting functions obtained within the present study [Eqs. (27)–(32)]. The LES data points suggest a neutral limit value smaller than unity, indicating that the transport of heat is more efficient than that of momentum, even under neutral conditions. However, we must take into account that there are only few LES data points in the near-neutral region for ϕ_h so that this estimate is not very certain. The value of Pr_t is then decreasing with decreasing stability of the flow, reaching approximately 0.15 near free-convective conditions. The turbulent transport of heat thus becomes more and more efficient compared to that of momentum. These findings are in line with recent studies. It is generally found that $\mathrm{Pr}_t \leq 1$ [for a summary of proposed values, see Foken (2006) and Li et al. (2015)]. Businger et al. (1971), for example, reported $\mathrm{Pr}_t \approx 0.74$ [or 0.95 in the correction for $\kappa = 0.4$ after Högström (1988)]. Li et al. (2012b) attributed the dependence on stability to interactions between turnover eddies and deviations in the temperature profile within their study. Recently, Li et al. (2015) showed that the dependence on stability is controlled by the ratio of Kolmogorov and Kolmogorov–Obukhov phenomenological constants as well as isotropization of turbulent flux production. Figure 4 also shows that the fitting functions (both the BD type and the new formulation) have problems capturing both the neutral limit as proposed by the LES data and the slope of Pr_t toward larger values of $-z/L$. This can be attributed to deficiencies in the fitting functions and the fact that they were determined independently. By using the least squares nonlinear regression, we can directly obtain an analytical formulation for $\mathrm{Pr}_t(z/L)$ from the LES data points, which reads

$$\mathrm{Pr}_t = 0.53\left(0.49 - 0.51\frac{z}{L}\right)^{-0.64}. \tag{34}$$

In the neutral limit of $-z/L \to 0$, this analytical function suggests $\mathrm{Pr}_t = 0.84$ (or $\mathrm{Pr}_t^{-1} = 1.19$), which is close to the new LES-based fitting functions ϕ_h and ϕ_m, which yield $\mathrm{Pr}_t = 0.79$. From the BD-type functions it follows that $\mathrm{Pr}_t = 1.0$ in the neutral limit. Generally we cannot observe a better representation of Pr_t than estimated from the new fitting functions ϕ_h and ϕ_m. The additional assumption commonly made for BD-type MOST function that $\phi_h = \phi_m^2$ implies that $\mathrm{Pr}_t = \phi_m \sim (z/L)^{-0.25}$. The analytical formulation based on the LES data gives $\mathrm{Pr}_t \sim (z/L)^{-0.64}$ and is thus obviously in contrast with this assumption.

c. *MOST relationships for standard deviations*

The nondimensional standard deviations of θ, q, and w were calculated analogous to the mean gradients. Please note that no data for σ_q were available for case W08 owing to a data loss.

1) Standard deviation of temperature and humidity

Figures 5a and 5b show the dimensionless standard deviations of temperature and humidity. They reveal remarkably little scatter so that all data points collapse to a single curve. The traditional fitting functions in literature follow a $-1/3$ power law. As for the mean gradients, the LES here suggests a steeper slope and rather follows -0.4. Both fitting functions are shown in Figs. 5a and 5b and read

$$\phi_{\sigma_\theta} = -2.1\left(1 - 9\frac{z}{L}\right)^{-1/3} \quad (-1/3\,\text{power law}), \tag{35}$$

$$\phi_{\sigma_\theta} = -1.2\left(0.2 - 1.7\frac{z}{L}\right)^{-0.4} \quad (\text{new}), \tag{36}$$

$$\phi_{\sigma_q} = -2.1\left(1 - 8\frac{z}{L}\right)^{-1/3} \quad (-1/3\,\text{power law}), \quad \text{and} \tag{37}$$

$$\phi_{\sigma_q} = -1.2\left(0.2 - 1.6\frac{z}{L}\right)^{-0.4} \quad (\text{new}). \tag{38}$$

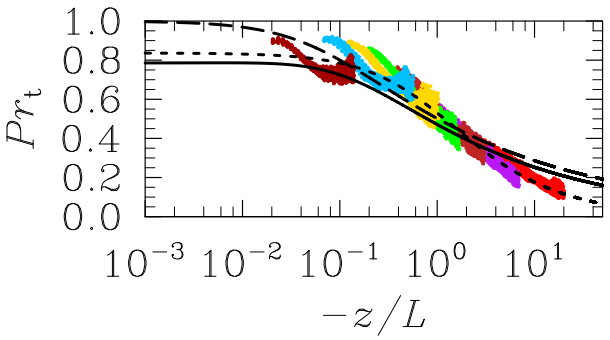

FIG. 4. Turbulent Prandtl number ($\mathrm{Pr}_t = \phi_h/\phi_m$), calculated from the LES data points for the MOST fitting functions given in Eqs. (27) and (28) and Eqs. (31) and (32). Colors and lines are as in Fig. 1. Additionally, an analytic fitting function according to Eq. (34) is given (short-dashed line).

Obviously, the assumption that $\phi_{\sigma_\theta} = \phi_{\sigma_q}$ is confirmed by the LES data. As for the mean gradients, we note that even the data from the free-convective case W00 follows MOST.

The comparison of the LES fittings with literature indicates that the fitting function with a $-1/3$ power law is within the range of the proposed functions (Figs. 6a,b). In particular, good agreement is found for ϕ_{σ_θ} and the function of Liu et al. (1998). The functions of Andreas et al. (1998) suggest somewhat higher values for both ϕ_{σ_θ} and ϕ_{σ_q} than found in the LES data. In principle the results obtained for the mean gradients are also valid for the standard deviations of temperature and humidity: the new LES fittings, with an adjusted power law deviate from the formerly proposed functions in literature, but they represent the LES data best.

2) STANDARD DEVIATION OF VERTICAL VELOCITY

The nondimensional standard deviation of vertical velocity in Fig. 5c reveals much less scatter than was found for the mean gradient of the horizontal wind velocity. Unlike all other dimensionless gradients and standard deviations, the LES data also follow the proposed 1/3 power law. A best-fit function is given by

$$\phi_{\sigma_w} = 1.0\left(1.0 - 4.1\frac{z}{L}\right)^{1/3}. \tag{39}$$

This function is also within the range of what is proposed from the analysis of former experimental data (see Fig. 6c; cf. Panofsky et al. 1977; Kaimal and Finnigan 1988; Andreas et al. 1998; Wilson 2008). It is noteworthy that the LES fit is very close to the function of Wilson (2008) (his type a).

d. Sensitivity analysis

In this section we aim at analyzing whether the results obtained so far (i.e., the new MOST functions based on LES data) are indeed universal, or whether effects of humidity, entrainment, or possibly of the surface Bowen ratio modify these functions. The latter would support the findings of some recent studies (McNaughton 2006; Wilson 2008; Li et al. 2012a) and the precursor of this paper (see M14).

Figure 7 shows the dimensionless data from case W08 as well as the data from the sensitivity runs as described in section 3b, complemented by the new LES-based fitting functions derived from the reference cases. For the mean gradients of temperature and humidity, as well as σ_θ and σ_w, we observe that all data points strictly follow the derived fitting functions and thus show no sensitivity. Neither differences in β_0 nor in the lapse rate affect the MOST functions. This also holds for the dry cases and we can hence argue that all quantities follow MOST and are most likely indeed universal. Furthermore, the mean wind gradient data display larger scatter, but all sensitivity simulations also follow the derived fitting function, which suggests that the previous statement can be extended to the horizontal wind speed.

It is seen that σ_q, however, displays a clear sensitivity to the lapse rate in the capping inversion (and thus to the entrainment of dry air). This does not come as a surprise as M14 had clearly demonstrated that C_q^2 was affected by entrainment and that in case W00_γ07 the spatial correlation coefficient between temperature and humidity rapidly decreased with height. As C_q^2 is a measure for the humidity variance of the turbulent eddies within the inertial subrange, it is reasonable to suspect that the variance itself should also display a sensitivity to the entrainment. In consequence, we thus conclude that ϕ_{σ_q} is not universal in situations when entrainment is significant. In that case, the assumption that $\phi_{\sigma_\theta} = \phi_{\sigma_q}$ does no longer hold. It is interesting that, unlike ϕ_{σ_q}, the mean gradient of humidity does not respond to the entrainment rate and appears to be universal. We attribute this finding to two circumstances. First, humidity is a rather passive quantity as it is mainly transported by turbulent eddies that are triggered by temperature differences and is, thus, caused by density fluctuations. The general effect of humidity on density is of course not negligible (as was shown by M14), but the effect of additional humidity fluctuations caused by entrainment is small compared to the effect of the background humidity on density. We can thus expect that the turbulent transport is not necessarily altered with a higher variance in humidity. Second, the variance itself is a measure of the structure of the humidity field, but it is not linked to the mean state. It also does not give information on the size of the structures

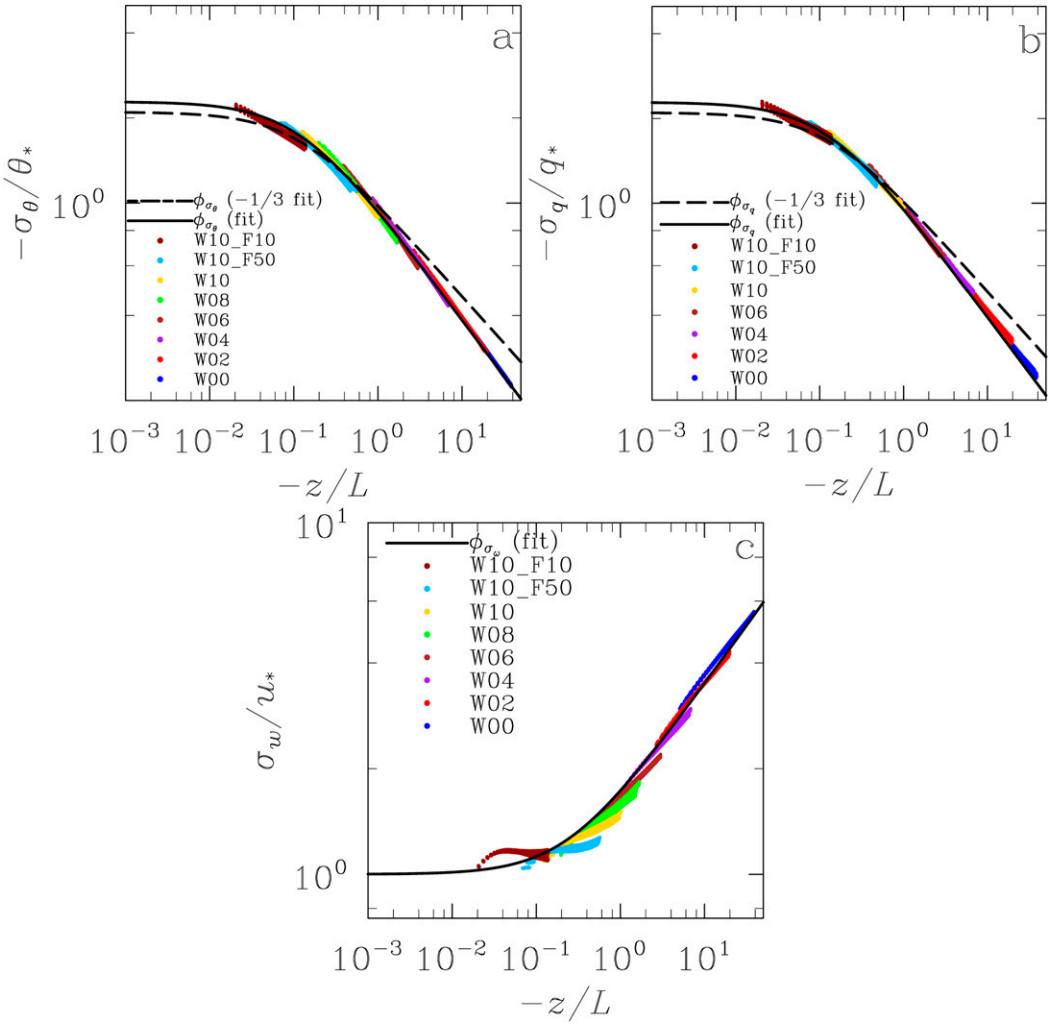

FIG. 5. Normalized standard deviations of (a) temperature, (b) humidity, and (c) the vertical velocity against stability parameter $-z/L$. The black solid lines indicate the determined MOST fitting functions ϕ, while the black dashed lines show the best fit with −1/3 slope.

responsible for the additional variance. The consequence of these circumstances is that the mean humidity gradient in our data is dominated by the near-surface stability and behaves according to MOST.

e. LFC scaling

The LFC constants A were calculated for the free-convection case W00 for all available time steps and height levels within the surface layer according to Eqs. (18)–(23). Figure 8 shows these data against height.

1) LFC CONSTANTS FOR MEAN GRADIENTS

From Figs. 8a and 8b a distinct height dependency in the nondimensional mean gradients is visible, with increasing values from the lowest levels to more or less constant values at $z \approx 20 - 60$ m and slightly increasing values above. A peak is visible at a height of 35 m, which was also found for structure parameters (see M14). As former studies had related such a peak to the subgrid-scale models used to derive the LFC constants (Khanna and Brasseur 1997; Brasseur and Wei 2010), M14 discussed that this peak shows no height dependence when altering the grid spacing. It is thus unlikely that it is related to the subgrid-scale model. A plausible explanation is the local shear-induced turbulence that is not considered in LFC scaling (Businger 1973) but that has the potential to alter the mean profiles. There seems also to be a slight time dependence, as the data cover a broader range of values at $z \approx 20 - 110$ m. However, variations in time and height lead to $A_\theta = A_q = -0.4 \pm 0.1$ (95% confidence interval), so that we can conclude that the scatter in the data is not

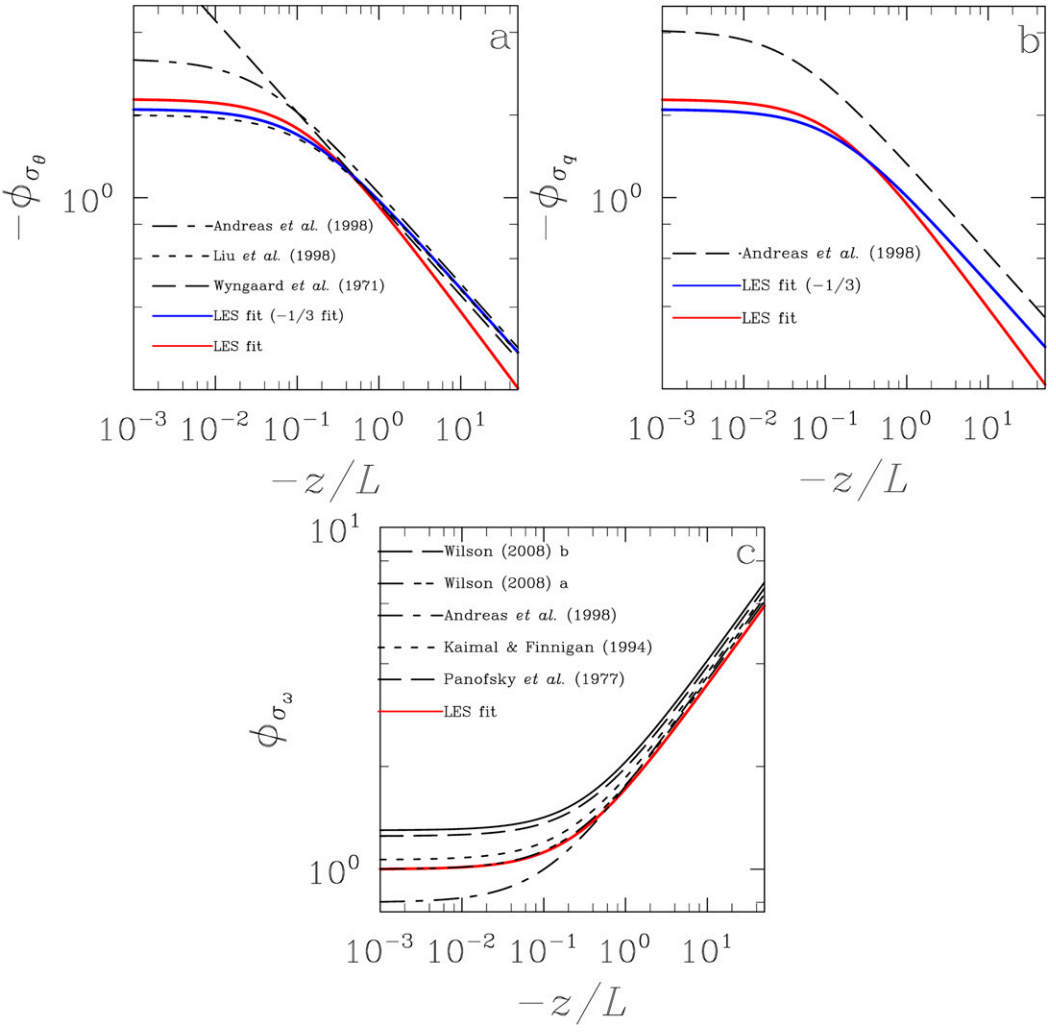

FIG. 6. Overview of fitting functions (a) ϕ_{σ_θ} and (b) ϕ_{σ_q}, and (c) ϕ_{σ_w} that have been proposed in literature against stability parameter $-z/L$ and compared to the LES fit (red solid lines) and the LES fit with $-1/3$ slope (solid blue lines). Probability density functions of $-z/L$ are as in Fig. 1 and are thus not shown here.

too large. The resulting value of -0.4 is close to -0.35 after Sorbjan (1986).

2) LFC CONSTANTS FOR STANDARD DEVIATIONS

As for the mean gradients, the normalized standard deviations also show a clear height dependence (see Figs. 8c–e). Unlike the mean gradients, however, we observe high values close to the surface and a decrease with height. We see also some scatter due to variability in time, which is apparently higher for σ_q than for σ_θ. The LES data suggest that $A_{\sigma_\theta} = 1.1 \pm 0.1$, $A_{\sigma_q} = 1.15 \pm 0.06$, and $A_{\sigma_w} = 1.24 \pm 0.04$. While the deviations from the mean are more pronounced for σ_θ (maximum deviation of 11%) and σ_q (maximum deviation of 9%), σ_w apparently displays only little scatter with deviations of not more than 3% from its mean. While we are not aware that any value for A_{σ_q} has been proposed in literature yet, we might assume that $A_{\sigma_q} \approx A_{\sigma_\theta}$, keeping in mind that there seems to be more scatter for humidity. For A_{σ_θ}, values between 1.29 and 1.41 have been reported (Wyngaard et al. 1971; Caughey and Readings 1975; Sorbjan 1986; Khanna and Brasseur 1997), which are slightly higher than what we found from our LES data (see also Table 3). For A_{σ_w}, values between 1.1 and 1.4 are suggested (Wyngaard et al. 1971; Caughey and Readings 1975; Sorbjan 1986; Shao and Hacker 1990). Our value of 1.24 is well amid this interval and very close to 1.26 reported by Sorbjan (1986).

Table 3 shows all LFC constants for the references and sensitivity cases, together with the estimates for standard deviations from MOST fitting functions, calculated by means of Eqs. (24)–(26). The MOST estimate

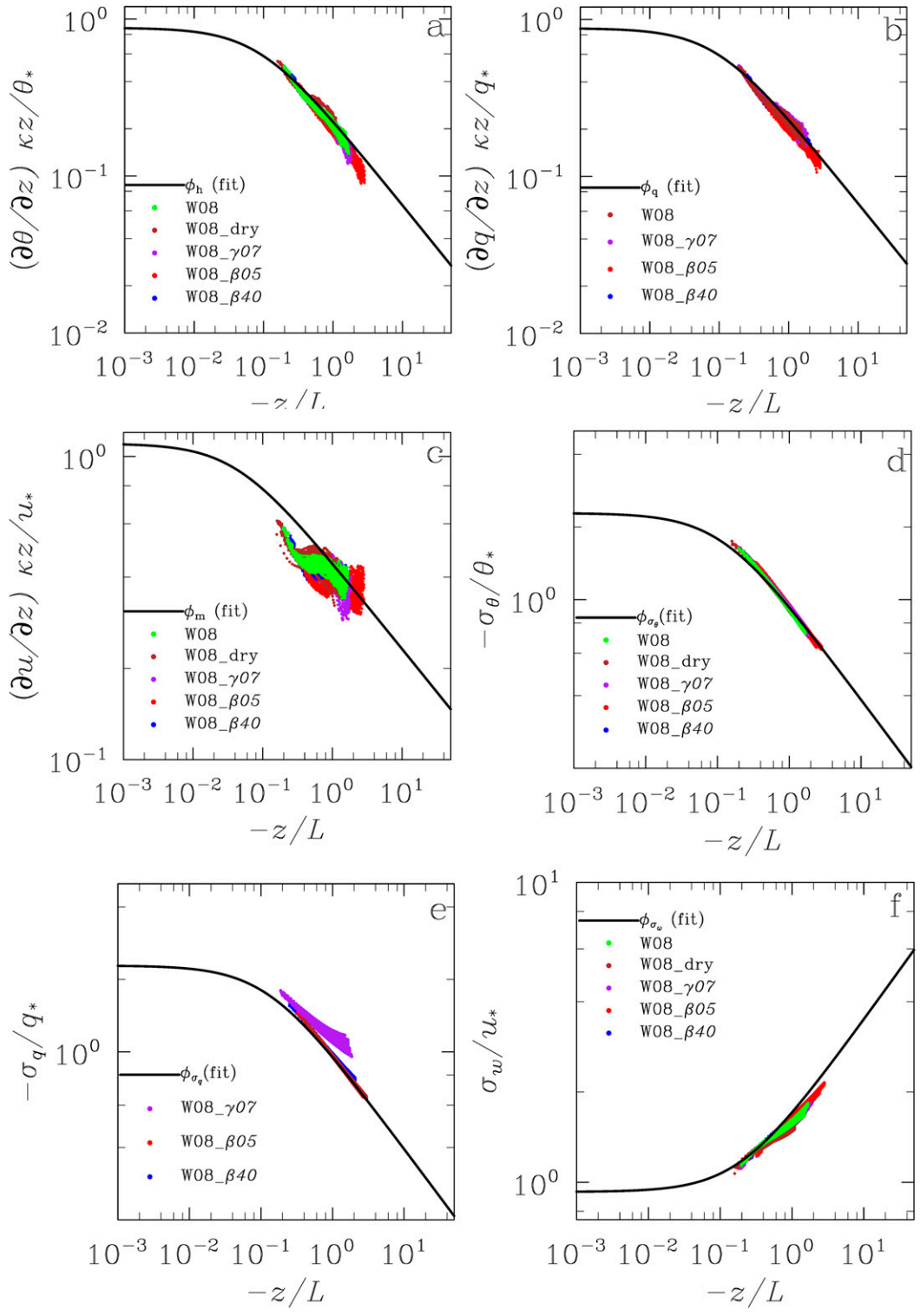

FIG. 7. Nondimensional mean gradients and standard deviations from sensitivity simulations and MOST fitting function (a) ϕ_θ, (b) ϕ_q, (c) ϕ_m, (d) ϕ_{σ_θ}, (e) ϕ_{σ_q}, and (f) ϕ_{σ_w}.

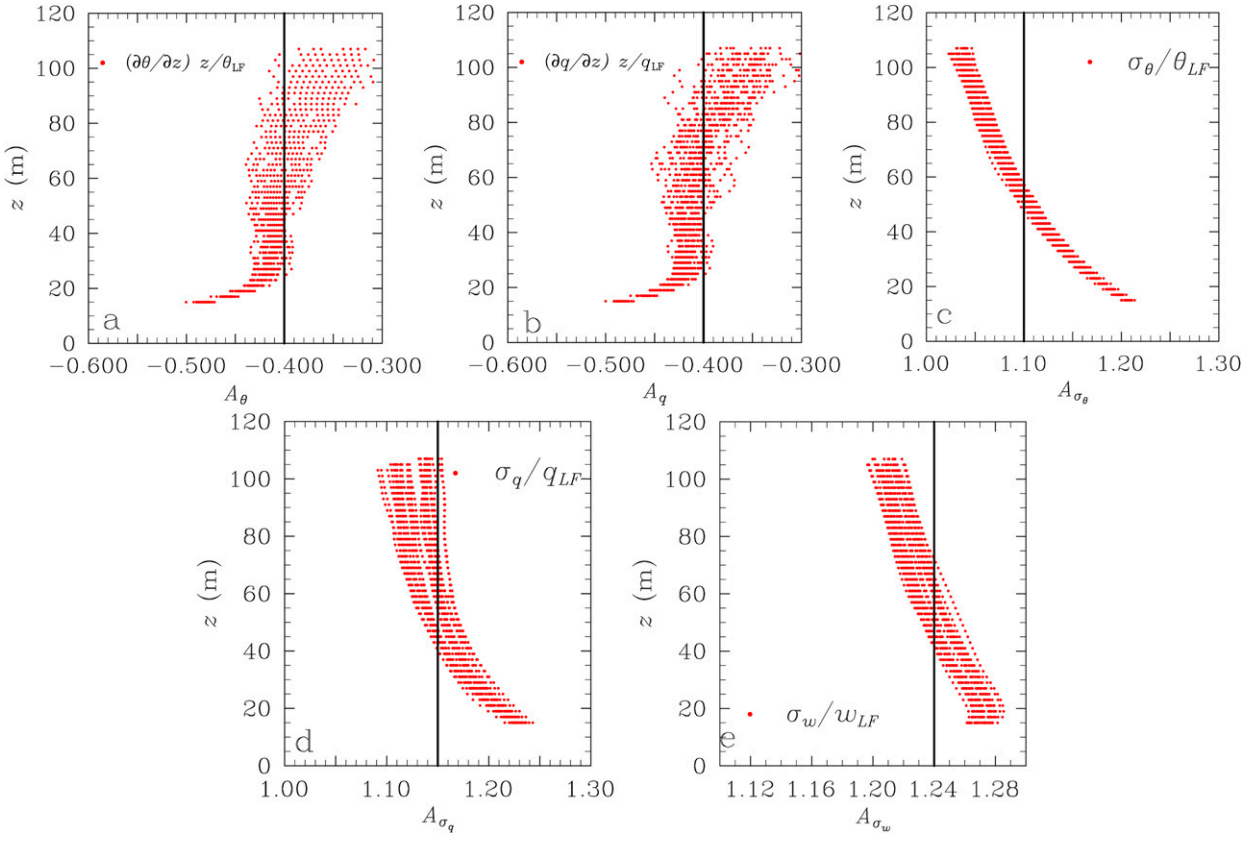

FIG. 8. Vertical profiles of (a) A_θ, (b) A_q, (c) A_{σ_θ}, (d) A_{σ_q}, and (e) A_{σ_w} in the lower unstable boundary layer for all available time steps.

of A_{σ_θ} (A_{σ_q}) is 1.37 (1.43) and therefore higher than 1.1 given by LFC scaling (see Table 3). However, it is well within the range of the proposed values from literature. For A_{σ_w}, the MOST fitting function predicts 1.18, which is a little smaller than 1.28 obtained from LFC scaling, but also within the range of the proposed values in literature. The large difference between the estimate from MOST fitting functions and LFC scaling for σ_θ can be explained by the fact, that the MOST fitting functions where shown to have deficiencies for large values of $-z/L$ and could thus not describe the behavior in the free-convection limit adequately. For A_{σ_w}, the MOST function followed the proposed slope from LFC scaling and is hence in much better agreement with the LFC prediction.

3) SENSITIVITY ANALYSIS

In analogy to the analysis in section 4d, the LFC constants were derived from the sensitivity cases (i.e., W00_dry, W00_β05, W00_β40, and W00_γ07). The results are shown in Table 3. It is striking that only A_{σ_q} is not constant for the sensitivity cases. More precisely, it has slightly higher values of 1.17 in case W00_β40 as well as a clearly higher value of 1.4 in case W00_γ07.

TABLE 3. Overview of similarity constants for LFC scaling and their double standard deviation (95% confidence interval), and the estimated values from the derived MOST fitting functions.

Case	β_0	A_θ	A_q	A_{σ_θ}	A_{σ_q}	A_{σ_w}
W00	0.27	-0.4 ± 0.1	-0.4 ± 0.1	1.1 ± 0.1	1.15 ± 0.06	1.24 ± 0.04
W00_dry	∞	-0.4 ± 0.1	—	1.1 ± 0.1	—	1.24 ± 0.05
W00_β05	0.05	-0.4 ± 0.1	-0.4 ± 0.1	1.1 ± 0.1	1.14 ± 0.06	1.24 ± 0.05
W00_β40	0.4	-0.4 ± 0.1	-0.4 ± 0.1	1.1 ± 0.1	1.17 ± 0.05	1.24 ± 0.05
W00_γ07	0.27	-0.4 ± 0.1	-0.4 ± 0.1	1.1 ± 0.1	1.40 ± 0.2	1.24 ± 0.05
MOST	0.27	—	—	1.37	1.43	1.18
Literature	—	−0.35	—	1.29–1.41	—	1.1–1.40

Also note that the scatter has significantly increased in the latter case. This supports the findings obtained from the sensitivity analysis for the MOST relationships that σ_q can be influenced considerable by entrainment of dry air.

5. Summary and conclusions

The present LES study focused on the derivation of MOST similarity relationships for mean gradients and standard deviations in the unstable atmospheric surface layer. A comprehensive dataset of surface-layer-resolving LES cases, covering convective to near-neutral boundary layers, that was previously used by M14 to derive similarity relationships for structure parameters was further investigated for this purpose.

The analysis of the MOST relationships showed that the dimensionless gradients of potential temperature and specific humidity strictly follow universal functions that only depend on stability (i.e., $-z/L$), as proposed by theory and previous experiments. The LES data revealed remarkably little scatter in the data for temperature and humidity, while more scatter was observed for wind data, in agreement with past LES research. Generally, a height dependence of the data was found that is possibly caused by effects of the subgrid-scale model used, or by the simple fact that the assumption of a constant flux layer made by MOST is only an approximation of the surface layer structure. A comparison with formerly proposed MOST functions revealed that the LES data followed slightly steeper slopes than proposed by the BD-type similarity functions. In contrast, rather large scatter was observed in the dimensionless mean gradient of the horizontal wind velocity, particularly for large values of $-z/L$. Moreover, a ''kink'' in the MOST functions was observed around $-z/L \approx 8$, where the slope adjusted according to the predicted value from LFC scaling. This implies as change in the slope from $-1/2$ to $-1/3$ for temperature and humidity and a change from $-1/4$ to 1/3 for horizontal wind. Our analysis demonstrated that the latter is responsible for the observed scatter in the data at large values of $-z/L > 8$. We hypothesize that this behavior was not observed before owing to lacking measurement data in this stability range close to free convection. All proposed similarity functions in literature thus seem to fail for $-z/L > 8$, which is near free-convective conditions. More elaborated functions are required to incorporate the change of the slope at $-z/L = 8$. Furthermore, we could confirm that the similarity functions for temperature and humidity can be considered to be the same. The fitting functions derived from the LES data compare reasonably well to the previously suggested functions in literature, even though they suggest somewhat smaller values of the dimensionless mean gradients.

By comparing the estimates of the mean gradients from the newly derived fitting functions with the ''true'' gradients derived from the LES data, we could exclude possible errors in the fitting functions due to spurious self-correlation. The relative error of the predicted mean gradients due to scatter in the data was found to be around 6% for temperature and humidity and 10% for wind.

For the dimensionless standard deviations of potential temperature, specific humidity, and vertical velocity, we found little scatter in the data but slightly steeper slopes of the fitting functions for temperature and humidity than given by the proposed $-1/3$ power law in literature. The vertical velocity, however, behaves as expected from theory and follows a 1/3 power law. The fitting functions derived from the LES data are within the range of the previously proposed functions in literature.

In the free-convection limit, LFC scaling is more appropriate and the similarity relationships should reduce to constants. For the mean gradients, these constants are A_θ and A_q for temperature and humidity, respectively (no constant exists for the wind as the mean wind collapses to zero in free convection). Here, the LES dataset suggests $A_\theta = A_q = -0.4 \pm 0.1$ (95% confidence interval), which is close to the suggested value of -0.35 by Sorbjan (1986). The uncertainty in A_θ and A_q was mainly caused by a height dependence in the data. A possible reason for this was discussed to be local shear production by the turbulence near the surface (Businger 1973). The constants for the standard deviations of temperature, humidity, and vertical velocity were found to be $A_{\sigma_\theta} = 1.1$, $A_{\sigma_q} = 1.15$, and $A_{\sigma_w} = 1.24$, respectively. The constants for temperature and humidity are thus a little bit lower than previous suggestions, while the constant for vertical velocity is close to the proposed value of 1.26 after Sorbjan (1986).

To study the universality of the derived MOST–LFC relationships, data from a sensitivity study were analyzed, where the surface Bowen ratio and the lapse rate in the capping inversion were varied. The analysis revealed that almost all similarity relationships appear to be universal and both mean gradients and standard deviations do follow MOST. It is generally found that the similarity relationships for temperature quantities are roughly equal to those for humidity quantities. The analysis for σ_q, however, indicates that MOST–LFC relationships are only valid if entrainment of dry air at the top of the mixed layer is sufficiently small, the latter hereby quantified by an absolute value of the entrainment flux ratio ≤ 0.6. With an entrainment flux ratio of 1, the entrained dry air manifests itself in the humidity

fluctuations within the surface layer. Consequently, MOST–LFC fails for σ_q. It was shown that the effect of entrainment of dry air had, however, no impact on the mean gradient of specific humidity. We explained this finding by two circumstances. First, the humidity transport near the surface is mainly passive (i.e., achieved by turbulence triggered by density fluctuations). The relative importance of additional small humidity fluctuations on density and stability, however, is small compared to the effect of the background mean humidity. Additional variance that is caused by entrainment of dry air thus may enter the surface layer, but it does not alter the density significantly. Second, humidity variance is a measure for the structure of the humidity field, but no indicator for the mean state and thus not directly linked to the mean humidity gradient. Our data clearly showed that the mean humidity profile has no sensitivity to additional variance in humidity.

In summary, our results confirm that the MOST and LFC scaling are suitable frameworks for practical modeling and measurement applications and that the LES technique is a useful addition to achieve a better understanding of the uncertainties induced by the assumptions of MOST that are often violated in nature. Moreover, we were able to show that the LFC predicted slopes for the MOST fitting functions of mean gradients do not compete with the slopes observed directly in measurement data and that this long-standing issue was most likely due to lacking data for large values of $-z/L$.

Despite the obvious violation of one assumption of MOST, the horizontal homogeneity of the flow, atmospheric models generally apply MOST even over very heterogeneous surface (e.g., Patton et al. 2005; Huang et al. 2009; Mironov and Sullivan 2016). Maronga et al. (2014) demonstrated that the use of MOST–LFC for structure parameters over heterogeneous terrain gave reliable estimates of the surface sensible heat flux. In a follow-up study we will more thoroughly investigate the MOST framework over heterogeneous terrain and whether effects of surface heterogeneity should be incorporated in the similarity relationships.

Also, the use of direct numerical simulations is a promising technique to gain a better understanding of the applicability of MOST in the atmospheric surface layer. In such simulations, the near-surface region can be better resolved and the technique does not suffer from limitations implied by the use of a subgrid-scale model when performing LES, particularly near the surface of the model.

Acknowledgments. First of all, we would like to emphasize the quality of the very helpful comments of the anonymous reviewers that identified deficiencies in our initial manuscript and who provided excellent ideas for further analysis of our data that entered the revised version. Moreover, we thank Siegfried Raasch, Dieter Etling, and Christoph Knigge (all at Leibniz Universität Hannover, Germany) for reading a draft of the manuscript and/or for various discussions on the topic. Most part of the analyses in this paper were done during a research visit of the first author at the Geophysical Institute at the University of Bergen in May 2016, for which financial support was provided by Leibniz Universität Hannover and the University of Bergen, which is gratefully acknowledged. The simulations conducted for this study were supported by the German Research Foundation (DFG) under Grants RA 617/20-1 and RA 617/20-3. All simulations were performed on the former SGI Altix ICE at The North-German Supercomputing Alliance (HLRN), Hannover/Berlin. NCL (NCAR 2013) has been used for data analysis and visualization.

REFERENCES

Andreas, E. L, 1988: Estimating C_n^2 over snow and sea ice from meteorological data. *J. Opt. Soc. Amer.*, **5**, 481–495, doi:10.1364/JOSAA.5.000481.

——, 1991: Using scintillation at two wavelengths to measure path-averaged heat fluxes in free convection. *Bound.-Layer Meteor.*, **54**, 167–182, doi:10.1007/BF00119418.

——, and B. B. Hicks, 2002: Comments on ''Critical test of the validity of Monin–Obukhov similarity during convective conditions.'' *J. Atmos. Sci.*, **59**, 2605–2607, doi:10.1175/1520-0469(2002)059<2605:COCTOT>2.0.CO;2.

——, R. J. Hill, J. R. Gosz, D. I. Moore, W. D. Otto, and A. D. Sarma, 1998: Statistics of surface-layer turbulence over terrain with metre-scale heterogeneity. *Bound.-Layer Meteor.*, **86**, 379–408, doi:10.1023/A:1000609131683.

Andren, A., A. R. Brown, J. Graf, P. J. Mason, C.-H. Moeng, F. T. M. Nieuwstadt, and U. Schumann, 1994: Large-eddy simulation of a neutrally stratified boundary layer: A comparison of four computer codes. *Quart. J. Roy. Meteor. Soc.*, **120**, 1457–1484, doi:10.1002/qj.49712052003.

Beyrich, F., R. D. Kouznetsov, J.-P. Leps, A. Lüdi, W. M. L. Meijninger, and U. Weisensee, 2005: Structure parameters for temperature and humidity from simultaneous eddy-covariance and scintillometer measurements. *Meteor. Z.*, **14**, 641–649, doi:10.1127/0941-2948/2005/0064.

Blackadar, A. K., 1997: *Turbulence and Diffusion in the Atmosphere*. Springer, 185 pp.

Braam, M., A. F. Moene, F. Beyrich, and A. A. M. Holtslag, 2014: Similarity relations for C_T^2 in the unstable atmospheric surface layer: Dependence on regression approach, observation height and stability range. *Bound.-Layer Meteor.*, **153**, 63–87, doi:10.1007/s10546-014-9938-y.

Brasseur, J. G., and T. Wei, 2010: Designing large-eddy simulation of the turbulent boundary layer to capture law-of-the-wall scaling. *Phys. Fluids*, **22**, 021303, doi:10.1063/1.3319073.

Businger, J. A., 1973: A note on free convection. *Bound.-Layer Meteor.*, **4**, 323–326, doi:10.1007/BF02265241.

——, J. C. Wyngaard, Y. Izumi, and E. F. Bradley, 1971: Flux-profile relationships in the atmospheric surface layer. *J. Atmos. Sci.*,

28, 181–189, doi:10.1175/1520-0469(1971)028<0181:FPRITA>2.0.CO;2.

Carl, D. M., T. C. Tarbell, and H. A. Panofsky, 1973: Profiles of wind and temperature from towers over homogeneous terrain. *J. Atmos. Sci.*, **30**, 788–794, doi:10.1175/1520-0469(1973)030<0788:POWATF>2.0.CO;2.

Caughey, S. J., and C. J. Readings, 1975: Turbulent fluctuations in convective conditions. *Quart. J. Roy. Meteor. Soc.*, **101**, 537–542, doi:10.1002/qj.49710142910.

Chung, D., and G. Matheou, 2012: Direct numerical simulation of stationary homogeneous stratified sheared turbulence. *J. Fluid Mech.*, **696**, 434–467, doi:10.1017/jfm.2012.59.

Deardorff, J. W., 1980: Stratocumulus-capped mixed layers derived from a three-dimensional model. *Bound.-Layer Meteor.*, **18**, 495–527, doi:10.1007/BF00119502.

de Arellano, J., B. Gioli, F. Miglietta, H. J. J. Jonker, H. K. Baltink, R. W. A. Hutjes, and A. A. M. Holtslag, 2004: Entrainment process of carbon dioxide in the atmospheric boundary layer. *J. Geophys. Res.*, **109**, D18110, doi:10.1029/2004JD004725.

Delage, Y., and C. Girard, 1992: Stability functions correct at the free convection limit and consistent for both the surface and Ekman layers. *Bound.-Layer Meteor.*, **58**, 19–31, doi:10.1007/BF00120749.

Dyer, A. J., 1974: A review of flux-profile relationships. *Bound.-Layer Meteor.*, **7**, 363–372, doi:10.1007/BF00240838.

——, and E. F. Bradley, 1982: An alternative analysis of flux-gradient relationships at the 1976 ITCE. *Bound.-Layer Meteor.*, **22**, 3–19, doi:10.1007/BF00128053.

Evans, J. G., D. D. McNeil, J. W. Finch, T. Murray, R. J. Harding, H. C. Ward, and A. Verhoef, 2012: Determination of turbulent heat fluxes using a large aperture scintillometer over undulating mixed agricultural terrain. *Agric. For. Meteor.*, **166–167**, 221–233, doi:10.1016/j.agrformet.2012.07.010.

Fairall, C. W., E. F. Bradley, D. P. Rogers, J. B. Edson, and G. S. Young, 1996: Bulk parameterization of air-sea fluxes for Tropical Ocean-Global Atmosphere Coupled-Ocean Atmosphere Response Experiment. *J. Geophys. Res.*, **101**, 3747–3764, doi:10.1029/95JC03205.

Foken, T., 2006: 50 years of the Monin–Obukhov similarity theory. *Bound.-Layer Meteor.*, **119**, 431–447, doi:10.1007/s10546-006-9048-6.

Hartogensis, O. K., and H. A. R. De Bruin, 2005: Monin–Obukhov similarity functions of the structure parameter of temperature and turbulent kinetic energy dissipation rate in the stable boundary layer. *Bound.-Layer Meteor.*, **116**, 253–276, doi:10.1007/s10546-004-2817-1.

Hill, R. J., 1989: Implications of Monin–Obukhov similarity theory for scalar quantities. *J. Atmos. Sci.*, **46**, 2236–2244, doi:10.1175/1520-0469(1989)046<2236:IOMSTF>2.0.CO;2.

Högström, U., 1988: Non-dimensional wind and temperature profiles in the atmospheric surface layer: A re-evaluation. *Bound.-Layer Meteor.*, **42**, 55–78, doi:10.1007/BF00119875.

——, 1996: Review of some basic characteristics of the atmospheric surface layer. *Bound.-Layer Meteor.*, **78**, 215–246, doi:10.1007/BF00120937.

Huang, J., X. Lee, and E. G. Patton, 2009: Dissimilarity of scalar transport in the convective boundary layer in inhomogeneous landscapes. *Bound.-Layer Meteor.*, **130**, 327–345, doi:10.1007/s10546-009-9356-8.

Johansson, C., A.-S. Smedman, U. Högström, J. G. Brasseur, and S. Khanna, 2001: Critical test of the validity of Monin–Obukhov similarity during convective conditions. *J. Atmos. Sci.*, **58**, 1549–1566, doi:10.1175/1520-0469(2001)058<1549:CTOTVO>2.0.CO;2.

——, ——, ——, and ——, 2002: Reply. *J. Atmos. Sci.*, **59**, 2608–2614, doi:10.1175/1520-0469(2002)059<2608:R>2.0.CO;2.

Kader, B. A., and A. M. Yaglom, 1990: Mean fields and fluctuation moments in unstably stratified turbulent boundary layers. *J. Fluid Mech.*, **212**, 637–662, doi:10.1017/S0022112090002129.

Kaimal, J. C., and J. J. Finnigan, 1988: *Atmospheric Boundary Layer Flows: Their Structure and Measurement*. Oxford University Press, 289 pp.

——, and J. C. Wyngaard, 1990: The Kansas and Minnesota experiments. *Bound.-Layer Meteor.*, **50**, 31–47, doi:10.1007/BF00120517.

——, ——, D. A. Haugen, O. R. Coté, Y. Izumi, S. J. Caughey, and C. J. Readings, 1976: Turbulence structure in the convective boundary layer. *J. Atmos. Sci.*, **33**, 2152–2169, doi:10.1175/1520-0469(1976)033<2152:TSITCB>2.0.CO;2.

Katul, G., D. Li, M. Chamecki, and E. Bou-Zeid, 2013: Mean scalar concentration profile in a sheared and thermally stratified atmospheric surface layer. *Phys. Rev.*, **87E**, 023004, doi:10.1103/PhysRevE.87.023004.

Kays, W., 1994: Turbulent Prandtl number—Where are we? *J. Heat Transfer*, **116**, 284–295, doi:10.1115/1.2911398.

Khanna, S., and J. G. Brasseur, 1997: Analysis of Monin–Obukhov similarity from large-eddy simulations. *J. Fluid Mech.*, **345**, 251–286, doi:10.1017/S0022112097006277.

Kohsiek, W., W. M. L. Meijninger, A. F. Moene, B. G. Heusinkveld, O. K. Hartogensis, W. C. A. M. Hillen, and H. A. R. De Bruin, 2002: An extra large aperture scintillometer for long range applications. *Bound.-Layer Meteor.*, **105**, 119–127, doi:10.1023/A:1019600908144.

Kooijmans, L., and O. K. Hartogensis, 2016: Surface-layer similarity functions for dissipation rate and structure parameters of temperature and humidity based on eleven field experiments. *Bound.-Layer Meteor.*, **160**, 501–527, doi:10.1007/s10546-016-0152-y.

Letzel, M. O., M. Krane, and S. Raasch, 2008: High resolution urban large-eddy simulation studies from street canyon to neighbourhood scale. *Atmos. Environ.*, **42**, 8770–8784, doi:10.1016/j.atmosenv.2008.08.001.

Li, D., E. Bou-Zeid, and H. A. R. De Bruin, 2012a: Monin–Obukhov similarity functions for the structure parameters of temperature and humidity. *Bound.-Layer Meteor.*, **145**, 45–67, doi:10.1007/s10546-011-9660-y.

——, G. G. Katul, and E. Bou-Zeid, 2012b: Mean velocity and temperature profiles in a sheared diabatic turbulent boundary layer. *Phys. Fluids*, **24**, 105105, doi:10.1063/1.4757660.

——, ——, and S. S. Zilitinkevich, 2015: Revisiting the turbulent Prandtl number in an idealized atmospheric surface layer. *J. Atmos. Sci.*, **72**, 2394–2410, doi:10.1175/JAS-D-14-0335.1.

Liu, X., O. Tuskamoto, T. Oikawa, and E. Ohtaki, 1998: A study of correlations of scalar quantities in the atmospheric surface layer. *Bound.-Layer Meteor.*, **87**, 499–508, doi:10.1023/A:1000947709324.

Maronga, B., 2014: Monin–Obukhov similarity functions for the structure parameters of temperature and humidity in the unstable surface layer: Results from high-resolution large-eddy simulations. *J. Atmos. Sci.*, **71**, 716–733, doi:10.1175/JAS-D-13-0135.1.

——, A. F. Moene, D. van Dinther, S. Raasch, F. C. Bosveld, and B. Gioli, 2013: Derivation of structure parameters of temperature and humidity in the convective boundary layer from large-eddy simulations and implications for the interpretation of scintillometer observations. *Bound.-Layer Meteor.*, **148**, 1–30, doi:10.1007/s10546-013-9801-6.

——, O. K. Hartogensis, S. Raasch, and F. Beyrich, 2014: The effect of surface heterogeneity on the structure parameters of temperature and specific humidity: A large-eddy simulation case study for the LITFASS-2003 experiment. *Bound.-Layer Meteor.*, **153**, 441–470, doi:10.1007/s10546-014-9955-x.

——, and Coauthors, 2015: The Parallelized Large-Eddy Simulation Model (PALM) version 4.0 for atmospheric and oceanic flows: Model formulation, recent developments, and future perspectives. *Geosci. Model Dev.*, **8**, 2515–2551, doi:10.5194/gmd-8-2515-2015.

McNaughton, K., 2006: On the kinematic energy budget of the unstable atmospheric surface layer. *Bound.-Layer Meteor.*, **118**, 83–189, doi:10.1007/s10546-005-3779-7.

Meijninger, W. M. L., F. Beyrich, A. Lüdi, W. Kohsiek, and H. A. R. De Bruin, 2006: Scintillometer-based turbulent fluxes of sensible and latent heat over a heterogeneous land surface—A contribution to LITFASS-2003. *Bound.-Layer Meteor.*, **121**, 89–110, doi:10.1007/s10546-005-9022-8.

Mironov, D. V., and P. P. Sullivan, 2016: Second-moment budgets and mixing intensity in the stably stratified atmospheric boundary layer over thermally heterogeneous surfaces. *J. Atmos. Sci.*, **73**, 449–464, doi:10.1175/JAS-D-15-0075.1.

Monin, A. S., and A. M. Obukhov, 1954: Basic laws of turbulent mixing in the atmosphere near the ground. *Tr. Akad. Nauk SSSR Geofiz. Inst.*, **24**, 163–187.

NCAR, 2013: The NCAR Command Language (version 6.1.2). UCAR/NCAR/CISL/VETS, doi:10.5065/D6WD3XH5.

Obukhov, A. M., 1971: Turbulence in an atmosphere with a non-uniform temperature. *Bound.-Layer Meteor.*, **2**, 7–29, doi:10.1007/BF00718085.

Panofsky, H. A., and J. A. Dutton, 1984: *Atmospheric Turbulence: Models and Methods for Engineering Applications*. John Wiley & Sons, 397 pp.

——, H. Tennekes, D. H. Lenschow, and J. C. Wyngaard, 1977: The characteristics of turbulent velocity components in the surface layer under convective conditions. *Bound.-Layer Meteor.*, **11**, 355–361, doi:10.1007/BF02186086.

Patton, E. G., P. P. Sullivan, and C.-H. Moeng, 2005: The influence of idealized heterogeneity on wet and dry planetary boundary layers coupled to the land surface. *J. Atmos. Sci.*, **62**, 2078–2097, doi:10.1175/JAS3465.1.

Peltier, L. J., and J. C. Wyngaard, 1995: Structure–function parameters in the convective boundary layer from large-eddy simulation. *J. Atmos. Sci.*, **52**, 3641–3660, doi:10.1175/1520-0469(1995)052<3641:SPITCB>2.0.CO;2.

Raasch, S., and M. Schröter, 2001: PALM—A large-eddy simulation model performing on massively parallel computers. *Meteor. Z.*, **10**, 363–372, doi:10.1127/0941-2948/2001/0010-0363.

——, and T. Franke, 2011: Structure and formation of dust devil–like vortices in the atmospheric boundary layer: A high-resolution numerical study. *J. Geophys. Res.*, **116**, D16120, doi:10.1029/2011JD016010.

Saiki, E. M., C.-H. Moeng, and P. P. Sullivan, 2000: Large-eddy simulation of the stably stratified planetary boundary layer. *Bound.-Layer Meteor.*, **95**, 1–30, doi:10.1023/A:1002428223156.

Schumann, U., 1988: Minimum friction velocity and heat transfer in the rough surface layer of a convective boundary layer. *Bound.-Layer Meteor.*, **44**, 311–326, doi:10.1007/BF00123019.

Shao, Y., and J. M. Hacker, 1990: Local similarity relationships in a horizontally inhomogeneous boundary layer. *Bound.-Layer Meteor.*, **52**, 17–40, doi:10.1007/BF00123176.

Sorbjan, Z., 1986: On similarity in the atmospheric boundary layer. *Bound.-Layer Meteor.*, **34**, 377–397, doi:10.1007/BF00120989.

Steeneveld, G. J., A. A. M. Holtslag, and H. A. R. DeBruin, 2005: Fluxes and gradients in the convective surface layer and the possible role of boundary-layer depth and entrainment flux. *Bound.-Layer Meteor.*, **116**, 237–252, doi:10.1007/s10546-004-2730-7.

Stull, R. B., 1988: *An Introduction to Boundary Layer Meteorology*. Kluwer Academic Publishers, 666 pp.

Sullivan, P. P., J. C. McWilliams, and C.-H. Moeng, 1994: A subgrid-scale model for large-eddy simulation of planetary boundary-layer flows. *Bound.-Layer Meteor.*, **71**, 247–276, doi:10.1007/BF00713741.

van de Wiel, B. J. H., A. F. Moene, W. H. De Ronde, and H. J. J. Jonker, 2008: Local similarity in the stable boundary layer and mixing-length approaches: Consistency of concepts. *Bound.-Layer Meteor.*, **128**, 103–116, doi:10.1007/s10546-008-9277-y.

Wicker, L. J., and W. C. Skamarock, 2002: Time-splitting methods for elastic models using forward time schemes. *Mon. Wea. Rev.*, **130**, 2088–2097, doi:10.1175/1520-0493(2002)130<2088:TSMFEM>2.0.CO;2.

Williamson, J. H., 1980: Low-storage Runge-Kutta schemes. *J. Comput. Phys.*, **35**, 48–56, doi:10.1016/0021-9991(80)90033-9.

Wilson, D. K., 2001: An alternative function for the wind and temperature gradients in unstable surface layers. *Bound.-Layer Meteor.*, **99**, 151–158, doi:10.1023/A:1018718707419.

Wilson, J. D., 2008: Monin-Obukhov functions for standard deviations. *Bound.-Layer Meteor.*, **129**, 353–369, doi:10.1007/s10546-008-9319-5.

Wyngaard, J. C., O. R. Coté, and Y. Izumi, 1971: Local free convection, similarity, and the budgets of shear stress and heat flux. *J. Atmos. Sci.*, **28**, 1171–1182, doi:10.1175/1520-0469(1971)028<1171:LFCSAT>2.0.CO;2.